

## 9. REACTIVE SCATTERING IN MOLECULAR BEAMS

D. R. HERSCHBACH

*Department of Chemistry, Harvard University,  
Cambridge, Massachusetts*

### CONTENTS

I. Experimental Methods and Results.....	322
A. Apparatus and Experimental Conditions.....	322
B. Angular Distribution Measurements.....	328
C. Magnetic Deflection Analysis.....	341
D. Velocity Analysis of Products.....	344
E. Electric Deflection Analysis.....	347
F. Summary and Discussion.....	356
II. Chemical Forces in Charge-Transfer Reactions.....	367
A. The Harpooning Mechanism.....	368
B. Correlation with Electronic Structure.....	379
References .....	388

*The atoms move in the void and catching each other up jostle together, and some recoil in any direction that may chance, and others become entangled with one another in various degrees according to the symmetry of their shapes and sizes and positions and order, and they remain together and thus the coming into being of composite things is effected.*

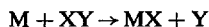
SIMPLICIUS (6th Century A.D.)

It has long been recognized that molecular beam experiments offer the most direct means to study the dynamics of elementary chemical reactions. In effect the time resolution is reduced to the duration of a single collision, of the order of  $10^{-13}$  sec. Thus, even quite primitive beam experiments can reveal the main features of the distribution of velocity vectors of the freshly formed product molecules and other properties inaccessible to traditional "bulb" methods of kinetics.

Until recently, chemical scattering experiments had yielded only meager results, and the small band of chemists who took up this work during the past decade was perhaps justly regarded as visionary. For a

method which depends so heavily on technology, an early period of evolutionary trauma had to be accepted. However, the newest developments, especially those of the past year, mark the end of this lean period, both in terms of experimental and theoretical methodology and in terms of results extensive enough to suggest chemical generalizations.

Reaction cross sections and angular distributions of both elastic and reactive scattering have now been measured for about twenty reactions of alkali metal atoms with halogen compounds which produce alkali halides,



The reactants XY include HX, RX, X<sub>2</sub>, XX', SX<sub>2</sub>, PX<sub>3</sub>, CH<sub>2</sub>X<sub>2</sub>, CHX<sub>3</sub>, CX<sub>4</sub>, SnX<sub>4</sub>, SF<sub>6</sub>, CF<sub>3</sub>I, and also NO<sub>2</sub> and RNO<sub>2</sub> (which form MO and MNO<sub>2</sub>). A complete summary is given in Table I (p. 357) and in the bibliography.<sup>1-52</sup> In a few cases, a direct velocity analysis of the MX product has been carried out. In others, the scattering has been subjected to analysis by inhomogeneous magnetic or electric deflecting fields. Mass spectrometric detection has also been employed, and it is expected that studies of reactions not involving alkali species will soon become feasible.

The theoretical apparatus required for detailed studies of reaction dynamics has also now reached working form. Until recently, the theory of scattering from a multidimensional potential-energy surface remained swaddled in formal theorems and the chemical implications of the reactive scattering experiments could only be discussed qualitatively. "Monte Carlo experiments" with computers have now opened up a new era for theoretical kinetics. As developed particularly by Bunker<sup>26,27</sup> and by Karplus,<sup>32,33</sup> these methods have made it feasible to examine vast numbers of exact trajectories for the general three-dimensional motion of a classical three-body system, without restrictive approximations. As yet, calculations have been reported for only one system (K + ICH<sub>3</sub>, with CH<sub>3</sub> treated as a mass point), but the results indicate that the principal features of the potential surface can be established within fairly narrow limits from the dynamical properties determined in the beam experiments. Simple phenomenological models of the type popular in nuclear physics have also been explored, particularly the "optical potential" model, and it is found that some of the dynamical features of the Monte Carlo calculations are nicely simulated by such models.

The scattering experiments have already established a beautifully simple pattern for the dynamics of alkali atom-halogen reactions. There has emerged a strong correlation among the magnitude of the total reaction cross section,  $\sigma_r$ , the preferred direction of recoil of the products, and the shape of the angular distribution of elastic scattering of the reactants. A *rebound* mechanism is found for reactions with "small" cross sections,  $\sigma_r \approx 10 \text{ \AA}^2$  (e.g., reactions with  $\text{CH}_3\text{I}$  and other alkyl iodides); most of the alkali halide product recoils into the *backward* hemisphere with respect to the incoming alkali atom beam and the elastic scattering is very similar to that of nonreactive molecules. A *stripping* mechanism is found for reactions with large cross sections,  $\sigma_r \approx 100 \text{ \AA}^2$  (e.g., reactions with  $\text{Br}_2$ ,  $\text{PBr}_3$ ,  $\text{CBr}_4$ , and many others): most of the alkali halide recoils *forward* and the elastic scattering falls off very rapidly at wide angles. A spectrum of intermediate cases is found as  $\sigma_r$  varies from the rebound to the stripping limit (e.g., reactions of various alkali metals with  $\text{CCl}_4$ ): the favored direction for recoil of the alkali halide gradually shifts from backwards to forwards and the falloff in the wide-angle elastic scattering becomes increasingly pronounced.

There are also several properties which hold regardless of the size of the reaction cross section. The total scattering (sum of elastically scattered M and reactively scattered MX) is very similar in both magnitude and angular distribution to that for nonreactive molecules of similar size and structure. Also, the anisotropy of the MX angular distributions indicates that both the rebound and stripping reactions proceed by a *direct* or *impulsive* mechanism; the duration of the reactive collisions must be very short, well below the average rotational period of a collision complex ( $\approx 5 \times 10^{-13}$  sec as a rough upper limit). For all the reactions, kinematic analysis of the reactive scattering indicates that the final relative translational kinetic energy of the products is comparable to the initial kinetic energy of the reactants, so that most of the chemical energy released appears as internal excitation of the products. As the electric deflection experiments have now demonstrated for several reactions that only a small part of this internal energy appears in rotation, most of it must be in vibrational excitation.

These general properties can all be accounted for by postulating that the reactions proceed via formation of an ion-pair,  $\text{M}^+ + \text{XY}^-$ . This "electron jump" model was proposed over thirty years ago to explain the large rate constants found in some of the Polanyi sodium flame

experiments, but not much could be done to test the model or to apply it elsewhere since knowledge of negative molecular ions has remained very scanty. Now, however, in addition to the evidence provided by the beam experiments, for many reactions it is possible to estimate the relevant potential curves for the  $XY^-$  ion by means of arguments developed for the analysis of charge-transfer spectra. Also, in some cases, use can be made of data and theory developed in recent electron-impact studies. In this way the chemical systematics associated with the transition from rebound to stripping behaviour and other details of the reaction dynamics can often be predicted by examining the electronic spectra and molecular orbital configuration of the reactant molecules  $XY$ . Simplicius would certainly have been very pleased with this.

Section I of this chapter illustrates the current status of experimental methods and summarizes the results which can be established directly from kinematic analysis of the data, without introducing theoretical models. The discussion is limited mainly to one prototype example, the  $K + Br_2$  reaction, for which the most detailed results are available. Section II celebrates the chemical implications. The qualitative correlation of spectra and reactivity implied by the electron jump mechanism is emphasized and some speculative features are pointed out which should be accessible to experimental test.

## I. EXPERIMENTAL METHODS AND RESULTS

As the early experiments and general aspects of the beam technique have been amply reviewed,<sup>3,15,16,21,47</sup> we shall illustrate here only the most important features of the recent reactive scattering studies carried out in our laboratory. Related work by other groups (at Birmingham, Oak Ridge, Brown, Wisconsin, and Bonn) receives only sporadic mention; however, Table I (in Section I-F) provides a complete listing of all the alkali reactions which have been studied in beams and a guide to the bibliography. In most essentials, the techniques employed in these experiments are derived from traditional practice of beam research in physics.<sup>53-55</sup> Many of the methods date back thirty or forty years, and our experience simply exemplifies the evolutionary principle, "Ontogeny Recapitulates Phylogeny."

### A. Apparatus and Experimental Conditions

Most of the experiments have been carried out with an almost rudimentary apparatus.<sup>15,24,38</sup> As shown in Figure 1, the beams are

formed by thermal effusion from ovens mounted on a turntable which is rotated to sweep the angular distribution past the detector. The angle of intersection of the beams can be varied from about  $60$  to  $135^\circ$  but is usually  $90^\circ$ . In the plane of the incident beams the accessible range of the scattering angle is  $\Theta = -60$  to  $150^\circ$  from the alkali beam. The out-of-plane scattering may be measured over a range of about  $\Phi = -10$  to  $+40^\circ$  by vertical adjustment of the sliding detector flange or over  $\Phi = -30$  to  $90^\circ$  by use of a special swivel mount for the detector.<sup>24</sup> In most of the experiments, the alkali metal beam was  $0.5^\circ$  wide and the gas beam  $12^\circ$  wide (full width at half intensity). The distance from the scattering center to the alkali oven is  $11$  cm, to the gas oven slit  $1.7$  cm, and to the detector usually about  $10$  cm. Use of a double-chamber oven for the alkali allows the temperature of the beam

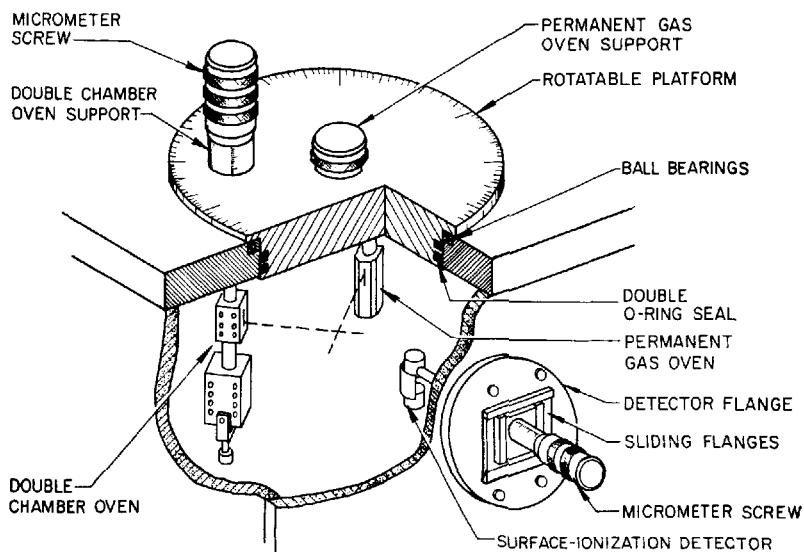


Fig. 1. Sketch of scattering chamber. Cold shields, collimating slits, shutters to interrupt the beams, and other details are omitted.

emerging from the upper chamber to be varied about  $300^\circ$  independently of the vapor pressure established in the lower chamber (about  $0.1$  mm Hg), which can then be maintained to provide the maximum intensity for effusive flow. The gas oven is connected to an external barostat

by a supply tube (not shown in Fig. 1) which passes through the support column in the rotating lid. Cold shields and collimating slits hide both ovens from the scattering center, and a cold shield also surrounds the detector. The entire scattering chamber is enclosed in a copper box attached to a large liquid nitrogen trap. For condensable reactants this provides a very high pumping speed (estimated as  $2 \times 10^5$  liters/sec) and although this apparatus lacks the customary differential pumping of the beam sources, the background pressure remains at about  $10^{-7}$  mm Hg during runs. As indicated in Figure 2, auxiliary equipment which surrounds the scattering chamber obscures somewhat the rudimentary character of the apparatus.

The detector must distinguish the reactively scattered MX molecules from the large background due to elastically scattered M atoms. A differential surface ionization technique was established by Taylor and Datz<sup>2,56</sup> in one of the early chemical scattering studies and this has been used in much of the subsequent work. Signals read on two surface ionization detectors are compared: one filament of tungsten or rhenium,<sup>57</sup> which is about equally sensitive to M and MX; the other a platinum-8% tungsten alloy, which under certain conditions is much more sensitive to M. For both M and MX, surface ionization produces  $M^+$  ions. The mechanism which inhibits surface ionization of alkali halides on platinum is not understood, but evidently it requires that the surface be suitably contaminated.<sup>57-59</sup> If the platinum filament is operated in a sufficiently "clean" vacuum, it appears to be very similar to tungsten in surface ionization properties.<sup>38,58</sup> Many materials are found to *poison* the response of the platinum filament, and this frustrated early attempts to study the reactions of alkali metals with many halogen compounds, including the diatomic halogen molecules.<sup>4,38</sup> The difficulty has been eliminated by means of a *prepoisoning* procedure<sup>38,39</sup> due to Touw and Trischka.<sup>59</sup> They demonstrated that two distinct and reproducible surface conditions of the platinum-8% tungsten alloy filament could be produced: Mode D, obtained by heating the wire in oxygen, detects both M and MX with high efficiency; Mode N, obtained by heating the wire in methane, is essentially nondetecting for MX. Measurements of the electron emission from the filament show that the overall work function is higher for Mode D than for Mode N and provide a convenient means to monitor the state of the surface. These two modes are found to remain immune to halogens for long periods of time.

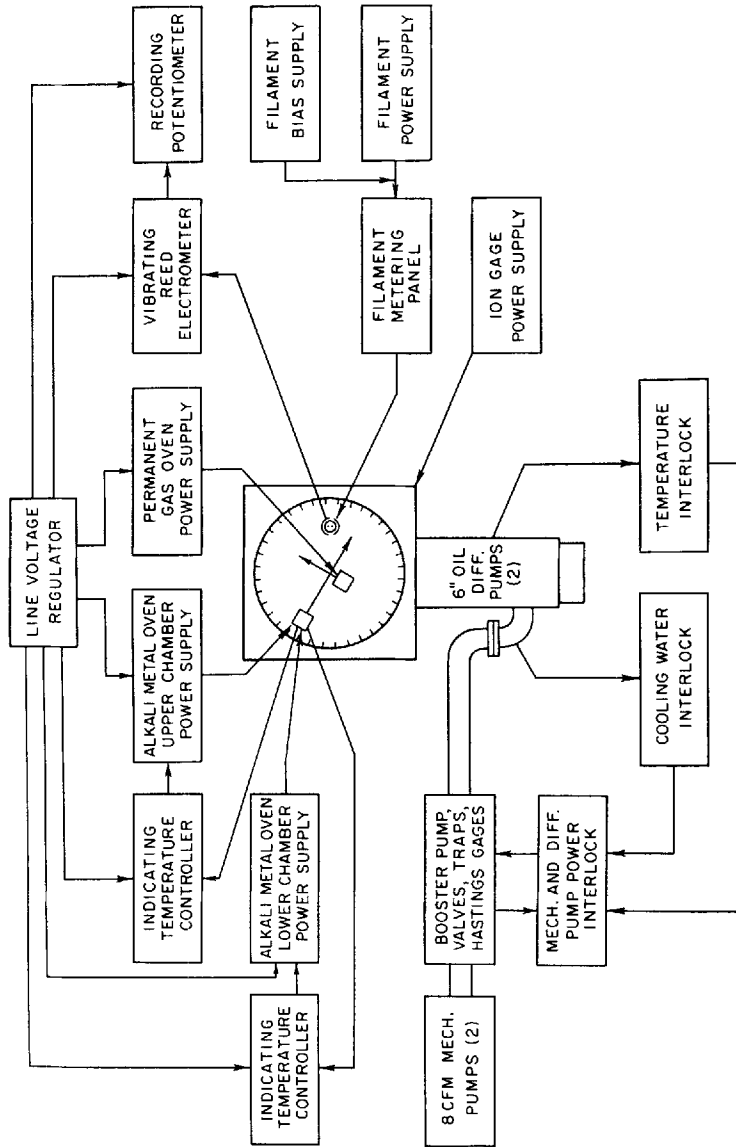


Fig. 2. Schematic diagram indicating auxiliary components of apparatus.

Recently, the detector flange shown in Figure 1 has been replaced with a side chamber in which the original detector is mounted behind one or the other of the analyzing elements pictured in Figure 3. In addition

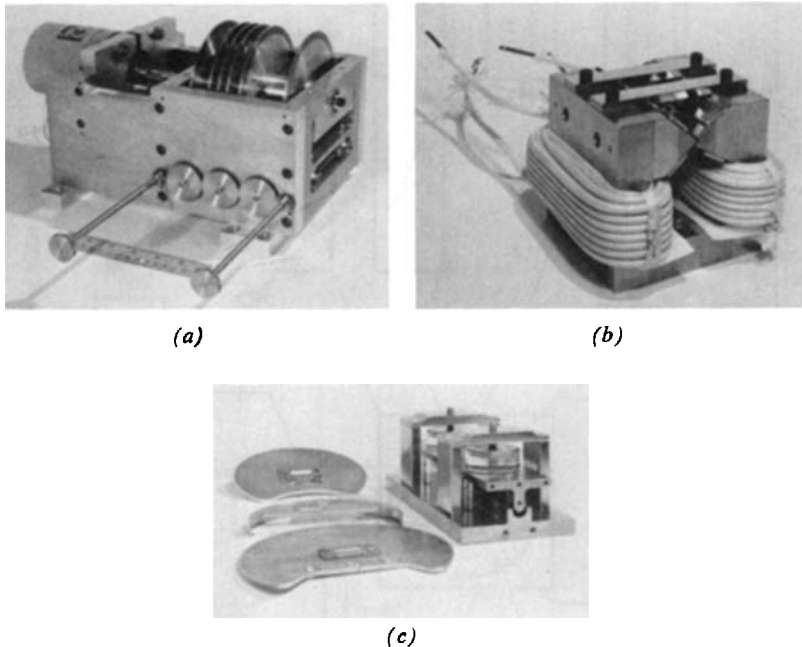


Fig. 3. Analyzing devices: (a) velocity selector; (b) inhomogeneous magnetic deflecting field; (c) inhomogeneous electric deflecting field. For (a), the distance between the first and last disk of the rotor is 10 cm; for (b) the field is 7 cm long and for (c) 15 cm.

to the spreading out of intensity imposed by the analysis, this reduces the solid angle subtended by the reaction volume at the detector by a factor of  $\sim 10^2$ – $10^3$ , since the distance is considerably increased (up to  $\sim 25$ – $30$  cm) and the analyzers require the use of narrow collimating slits ( $\sim 0.005$  cm for the velocity selector and  $0.001$  cm for the magnetic and electric fields). The loss in signal has been largely compensated by decreasing the detector noise level and by increasing the M atom beam flux. The noise from alkali metal impurities which previously had limited the detectable signal has been greatly reduced by the use of single-crystal tungsten filaments.<sup>60</sup> Signals as low as  $3 \times 10^{-16}$  A (2000

particles/sec) are now measurable. Another improvement of at least one order of magnitude could be obtained by use of beam modulation.<sup>61</sup> The flux increase has come from abandoning the traditional effusive flow conditions. The alkali oven is now equipped with thick slits shaped to conform to hydrodynamic criteria and the oven is operated at pressures up to 50-fold higher ( $\sim 20$  mm Hg) than allowed for effusive flow. The emergent beam is far from the mythical collision-free condition, but the scattering which occurs within the beam endows it with a "self-purifying" property. Measurements with the analyzers indicate that after traveling a few centimeters the beam approaches effusive flow. This simple method provides a tenfold or greater enhancement in intensity and a considerably narrower velocity distribution, and represents a modest step towards the supersonic jet or "Laval nozzle" technique which has been intensively developed during the past few years by chemical engineers.<sup>62</sup> It was first successfully applied to alkali beams by the Bonn group.<sup>63</sup>

The inhomogeneous magnetic deflecting field has been used to eliminate most of the background signal due to the paramagnetic M atoms and thus obtain a direct measurement of the distribution of the diamagnetic MX molecules.<sup>31</sup> With this the results derived from the modified differential surface ionization method have been verified for several reactions; also, measurements of the MX angular distributions have been much improved in the small-angle scattering region, which previously was almost inaccessible because the M atom background is very large there.

Since the velocity selector and electric deflecting field provide other means to sort atoms from molecules, as an incidental aspect of their function as analyzers, they also extend significantly the scope of the detection method. In the study of reactions of alkali atoms with  $\text{NO}_2$ , for example, the differential surface ionization method was unsuccessful.<sup>38,45</sup> Despite drastic efforts, the Pt-W filament could not be made to operate in the nondetecting mode; even the very low ambient concentration of  $\text{NO}_2$  appears to be sufficient to stabilize the filament in the detecting mode. Use of the magnetic field also failed to separate the product, as practically the whole scattered signal was found to be paramagnetic. However, the electric field revealed that the reaction actually produces a large yield of polar molecules.<sup>45</sup> These deflection experiments show that the product is almost certainly the MO molecule (which until very recently had not been observed spectroscopically<sup>64</sup>).

A few preliminary experiments have been carried out with a Paul mass filter and ion multiplier behind the surface ionization detectors; this has made possible the study of reactions such as  $\text{Rb} + \text{NaI} \rightarrow \text{RbI} + \text{Na}$ , which involve two different alkali metal atoms.<sup>38</sup>

In typical angular distribution experiments (made without the use of the analyzer devices or the Laval slits), the concentration of M atoms within the volume defined by the intersection of the beams is about  $10^{10}$  atoms/cm<sup>3</sup>, equivalent to a pressure of  $10^{-6}$  mm Hg, and that of the gas molecules is about 100-fold greater. About  $10^{14}$  M atoms/sec enter the reaction volume, of which roughly 0.1–1% react to form MX while about 10% undergo elastic scattering. The steady-state concentration of MX in the reaction volume is roughly  $10^7$ – $10^8$  molecules/cm<sup>3</sup>, the pressure  $10^{-9}$ – $10^{-8}$  mm Hg. At the peak of the MX angular distribution, about  $10^{10}$ – $10^{11}$  molecules/cm<sup>2</sup>/sec arrive at the detector; for many of the reactions studied more than a month would be required to deposit a monolayer of MX molecules.

### B. Angular Distribution Measurements

In reactive scattering experiments the object is to determine the direction and magnitude of the *recoil* velocity vectors  $\mathbf{u}$  that carry the products away from the center-of-mass, which proceeds with constant velocity  $\mathbf{C}$  regardless of the outcome of the collision. However, the observable spectrum of laboratory velocity vectors is a *vector sum*,  $\mathbf{v} = \mathbf{u} + \mathbf{C}$ . In the laboratory spectrum the (unknown) distributions in the recoil angle and energy therefore are usually strongly coupled and also may be drastically blurred by the (known) distribution in  $\mathbf{C}$  vectors which arises from the spread in initial conditions. For systems with favorable kinematics it is nonetheless often possible to establish some of the main qualitative features of the recoil spectrum from laboratory angular distribution measurements, without resorting to velocity analysis of either reactants or products. This is so because in thermal energy crossed beam experiments the reactants usually have comparable velocities and the  $\mathbf{C}$  velocity vector points sideways, at a wide angle intermediate between the directions of the incident beams. A rough measure of the recoil spectrum of a product thus may be obtained simply from the displacement of its laboratory angular distribution from the calculated distribution of  $\mathbf{C}$  vectors.

This primitive method has now been used in many reactive scattering studies (see Table I). The kinematic analysis and results have been

discussed in detail in other reviews.<sup>15,47</sup> The method was first applied to  $K + CH_3I$  and other alkyl iodide reactions.<sup>7,15</sup> It was found that the laboratory distribution (LAB, or  $v_{KI}$  distribution) of the KI product shows a broad peak at a wide angle (near  $\Theta \sim 85^\circ$ , measured from the direction of the parent K beam, see Fig. 6), well beyond the peak in the distribution of C vectors (which is near  $\Theta \sim 50^\circ$ ). The kinematic analysis of the LAB distribution demonstrated that in the center-of-mass reference system (CM, or  $u_{KI}$  distribution) most of the KI must recoil into the *backward* hemisphere with respect to the incoming K atoms (see Fig. 9). This is characteristic of what is now called the *rebound* mechanism.<sup>47,48,50</sup> The kinematic analysis also provided a rough estimate of the magnitude of the most probable  $u_{KI}$  recoil vector. Since this is quite small ( $\sim 100$ – $200$  m/sec), only a small part of the chemical energy released in the reaction (roughly 2–5 kcal/mole out of about 25 kcal/mole) can appear in the final relative translational motion of KI and  $CH_3$ ; most of the energy must be present as vibrational or rotational excitation of the products.

Figures 4 and 5 illustrate the results obtained in a similar study<sup>38,39</sup> of the  $K + Br_2$  reaction, which proved to be a prototype example of the *stripping* mechanism.<sup>28,39,42,47</sup> Here most of the KBr recoils into the *forward* hemisphere with respect to the incident K atoms, although again only a small fraction of the energy released appears in translational motion of the products.

The reaction yield is remarkably large. As illustrated by the primary data of Figure 4, the angular distribution of the *total scattering* (sum of K and KBr, as measured on the W filament or the Pt-W alloy in the "detecting" mode) shows a relatively gradual falloff at wide angles, whereas the *elastic scattering* (K intensity, as measured on the Pt-W filament in the "nondetecting" mode) falls off very rapidly. Note that the ordinate scale is logarithmic. Beyond  $\Theta \approx \pm 30^\circ$  the KBr intensity is roughly an order-of-magnitude larger than the K signal, in contrast to the situation found for rebound reactions (see Fig. 11), where the reactive scattering is always accompanied by a comparable amount of elastic scattering. The nominal yield (integrated intensity of KBr divided by total K scattered from the parent beam) derived from Figure 4 is  $\sim 10\%$ , and this does not include the contribution from the out-of-plane scattering which misses the detector. The reaction cross section is thus  $\approx 10\%$  of the total beam-scattering cross section (compared with only  $\sim 0.5\%$  for the  $K + CH_3I$  case), or roughly  $\approx 100 \text{ \AA}^2$ .

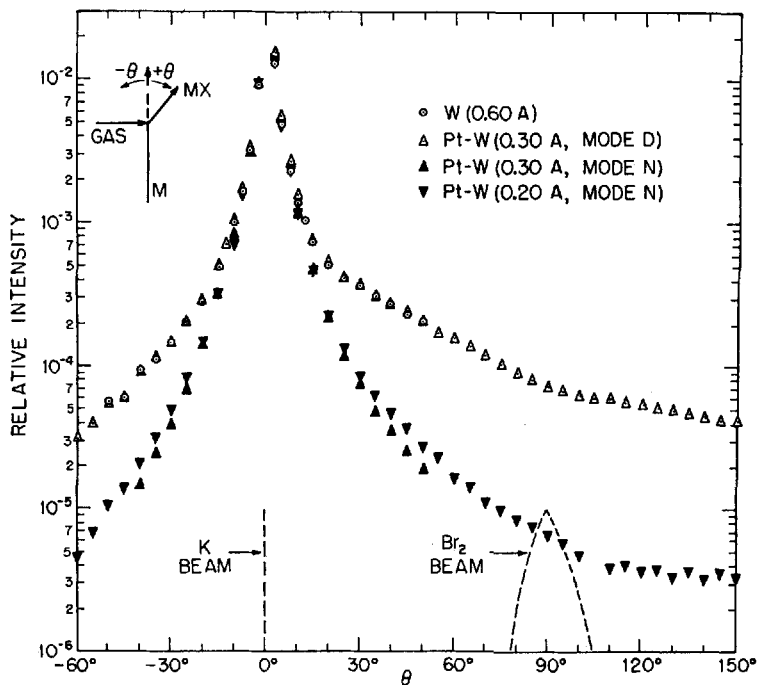


Fig. 4. Scattering of  $K + Br_2$  measured on various surface ionization filaments. The ordinate scale gives the ratio of the actual signal to the attenuation of the parent  $K$  beam measured on the same filament. Readings on the  $W$  filament ( $\circ$ ) or the  $Pt-W$  filament in the "detecting" mode ( $\Delta$ ) indicate the sum of scattered  $K$  and  $KBr$ ; readings on  $Pt-W$  in the "nondetecting" mode ( $\blacktriangle$ ) indicate scattered  $K$  atoms.

Figure 5 shows the angular distribution of  $KBr$  and the main features of the kinematic analysis. The  $KBr$  relative intensity is derived by subtracting the mode  $N$  detector signal from the mode  $D$  result and dividing by the attenuation of the parent  $K$  beam. Outside the region  $\Theta \approx \pm 20^\circ$  the subtraction is a small or negligible correction, but the uncertainty becomes large at small angles and points within  $\Theta \approx 5^\circ$  had to be discarded. The experimental points shown are the average of three separate runs, and the error bars indicate the standard deviation. Although the precise location of the peak remains uncertain by a few degrees, the general form is well determined and has been verified closely in the magnetic deflection experiments (see Fig. 11).

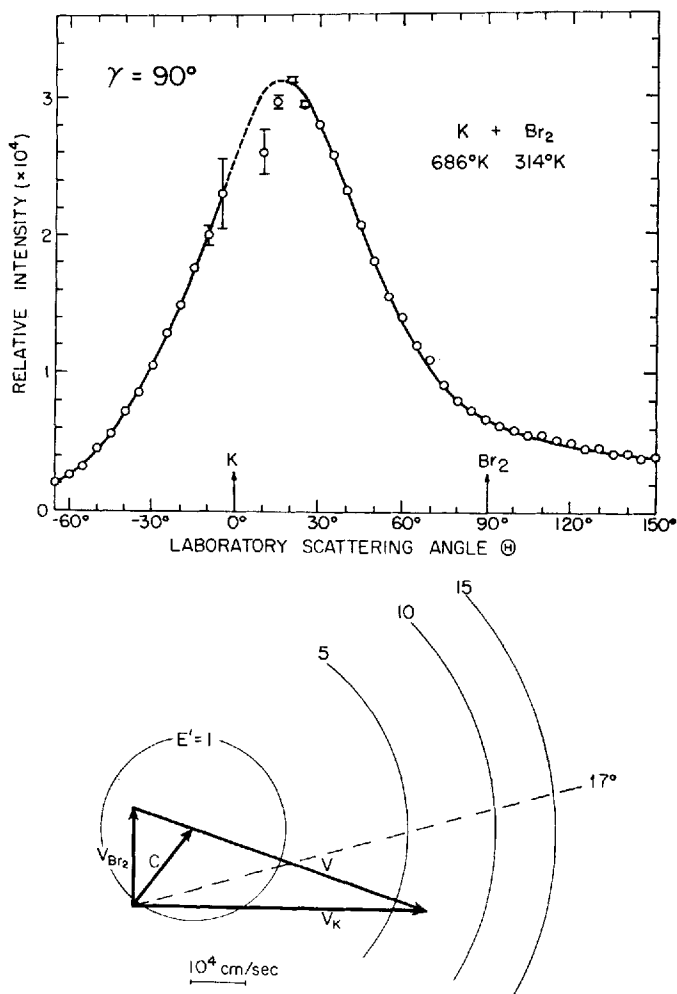


Fig. 5. Laboratory angular distribution of KBr from the  $\text{K} + \text{Br}_2$  reaction (measured in the plane of the incident beams). The lower panel gives the kinematic diagram corresponding to the most probable velocities in the reactant beams; the circles indicate the length of recoil velocity vectors for KBr produced with various amounts of final relative translational kinetic energy  $E'$  (kcal/mole).

The kinematic analysis consists of comparing the observed product distribution with the spectrum of recoil vectors allowed by the conservation laws for energy and linear momentum.<sup>10,15,50</sup> Newtonian mechanics is rigorously applicable here. In quantum mechanics, the velocity vectors in the asymptotic initial and final states of a collision are subject to the same, essentially geometrical relationships; in these asymptotic translational states the beam particles are too far apart to interact, hence need not be precisely localized in space and can be assigned definite momenta despite Heisenberg's principle.

The qualitative features may be seen from the vector diagram given in the lower part of Figure 5, which we like to call a *Newton diagram*. The most probable velocity vectors in the reactant beams are shown;  $\mathbf{V}$  denotes the *initial* relative velocity vector and  $\mathbf{C}$  is the center-of-mass vector. As required by momentum balance, the tip of  $\mathbf{C}$  partitions  $\mathbf{V}$  into segments having lengths in the inverse ratio of the masses of the reactant molecules. The recoil velocity vectors of the products,  $\mathbf{u} = \mathbf{v} - \mathbf{C}$ , are likewise related to the *final* relative velocity vector  $\mathbf{V}'$  by

$$\mathbf{u}_1 = (m_2/M)\mathbf{V}' \quad \mathbf{u}_2 = -(m_1/M)\mathbf{V}' \quad (1)$$

where  $1 \leftrightarrow \text{Br}$ ,  $2 \leftrightarrow \text{KBr}$ , and  $M$  is the total mass. The  $\mathbf{V}'$  vector may take any direction, but energy conservation restricts its magnitude. The total energy available to the reaction products is

$$E' + W' = E + W + \Delta D_0 \quad (2)$$

where  $E = \frac{1}{2}\mu V^2$  and  $E' = \frac{1}{2}\mu' V'^2$  are the initial and final relative translational kinetic energy ( $\mu$  and  $\mu'$  are the reduced masses),  $W$  and  $W'$  denote the internal excitation of the reactants and products, respectively, and  $\Delta D_0$  is the difference in dissociation energies of the new and old bonds (measured from the zero-point vibrational levels). For the  $\text{K} + \text{Br}_2$  reaction, the chemical energy released is  $\Delta D_0 \simeq 45$  kcal/mole; the thermal distribution of initial relative kinetic energy is peaked at  $E = 1.2$  kcal/mole; and the  $\text{Br}_2$  is mostly (77%) in the ground vibrational state with a rotational distribution peaked near  $W = 0.3$  kcal/mole (18% has an additional 0.9 kcal/mole in thermal excitation of the first vibrational state). Thus the possible spectrum of recoil vectors for KBr is represented by a set of spheres about the tip of  $\mathbf{C}$ , constructed from Eqs. (1) and (2), one for each value accessible to  $E'$  up to the maximum of about 48 kcal/mole.

From Figure 5 it is apparent that in order for the peak to appear near  $\Theta \sim 17^\circ$  in the LAB distribution, much of the KBr must recoil forward

(and the Br backward) in the CM distribution. A rough, *nominal* value of the recoil energy  $E'$  may be estimated by assuming that the KBr recoils directly forward along  $\mathbf{V}$ ; this gives  $E' \sim 1$  kcal/mole and accordingly the internal excitation  $W' \sim 45$  kcal/mole. This rather cavalier procedure has proven surprisingly useful. The nominal  $E'$  is also near 1 kcal/mole for many of the other reactions studied and often the shifts in the position of the LAB peak caused by changing either the angle of intersection or the temperature of the reactant beams are very close to predictions obtained from the nominal analysis. However, there is considerable leeway in the quantitative kinematic interpretation. Detailed calculations must be carried out to make allowance for distributions in both the recoil angle and energy and the blurring effect of the velocity distributions in the reactant beams.<sup>42,50</sup> Two features provide stringent requirements in deciding the *range* of recoil vectors compatible with the data. The scattering must have cylindrical symmetry about  $\mathbf{V}$ , since the incident beams contain all possible molecular orientations and impact parameters. Also, an acceptable recoil distribution must conform to the Jacobian factor for the LAB  $\leftrightarrow$  CM angle transformation, which often introduces severe distortions in the laboratory "image" of the recoil spectrum. Comparisons of the data with extensive trial calculations<sup>42,65</sup> (see Fig. 9, for example) indicate that for  $\text{K} + \text{Br}_2$  at least 50% of the reactive scattering must come from recoil angles within  $\pm 45^\circ$  of the direction of  $\mathbf{V}$  and recoil energy  $E' \sim 0.3$  to 10 kcal/mole (or  $W' \lesssim 35$  kcal/mole).

Much of the uncertainty is inherent in the kinematic analysis and arises from freedom in adjusting the distributions of both recoil angle and energy rather than from the velocity averaging. For the  $\text{Cs} + \text{Br}_2$  reaction, a study using velocity selection of the Cs beam has been carried out at Oak Ridge.<sup>28</sup> As the Cs velocity varied from 300 to 450 cm/sec, the CsBr peak was found to shift to slightly smaller angles (from  $22^\circ$  to  $18^\circ$ ) and to decrease appreciably in width (from  $46^\circ$  to  $33^\circ$  in the full width at half-intensity). These variations are closely simulated by a calculation which assumes the recoil is strictly forward along  $\mathbf{V}$  with  $E'/E = 0.3$  and averages a set of appropriate kinematic diagrams over the velocity distribution in the  $\text{Br}_2$  beam. Although this calculation also accounts for about 60% of the observed width of the CsBr peaks, calculations which allow distributions in both angle and energy show that the range of recoil spectra compatible with the data is in this case nearly as broad as in the experiments without velocity selection.

Further aspects of the angular distribution studies are illustrated in Figures 6-9, which compare the results for prototype stripping and rebound reactions. The LAB distributions for the  $K + ICl$  and  $K + CH_3I$  systems are shown in Figures 6 and 7. Although the results for  $ICl$  and  $Br_2$  are practically the same,  $ICl$  is chosen as the stripping example here since it offers a closer kinematic and chemical analogy to  $CH_3I$ . It is not possible to decide whether  $K + ICl$  yields mainly  $KI + Cl$  or  $KCl + I$  from analysis of the product distribution, however.<sup>47,49</sup> Figure 6 shows product distributions measured in successive runs with the same experimental conditions. As before, the ordinate scale gives the ratio of the product signal to the attenuation of the parent  $K$  beam; since the total scattering cross sections (determined essentially just by the van der Waals forces) are nearly the same for  $ICl$  and  $CH_3I$ , this normalization allows a direct comparison of the reaction yields. Note that not only is the total yield much greater for the stripping case, but even the scattering which corresponds to backward recoil in the CM system (which appears in the region  $60-150^\circ$  in the LAB distribution) is substantially larger than for the rebound case. Figure 7 brings out another striking property. Whereas the stripping and rebound cases show drastic differences in both reactive and nonreactive scattering, the *total* scattering is very similar in both magnitude and angular distribution.

In Figures 8 and 9 the comparisons are made in terms of CM angular distributions derived from an approximate kinematic analysis. Since in the CM system the results for various stripping reactions are very similar,  $Br_2$  is again taken as the example. Figure 8 gives results for nonreactive scattering. The LAB intensity distributions measured on the Pt-W alloy filament in mode N were transformed to the CM system, multiplied by  $\sin \theta_{CM}$  in order to remove the form factor due to the solid-angle element in the differential cross section, and normalized in the small-angle region where the patterns should be perturbed negligibly by reactive scattering. The kinematic relations appropriate for the most probable velocities in the parent beams were used in carrying out the transformation to the CM system. It has been shown<sup>22,65</sup> that in the case of elastic scattering of a beam of fast light atoms from slow heavy molecules this procedure yields a close approximation to the average of the CM angular distribution over the distribution of relative kinetic energy. The heavy dashed curve shows the averaged distribution calculated<sup>22</sup> for elastic scattering produced by an Exp-6

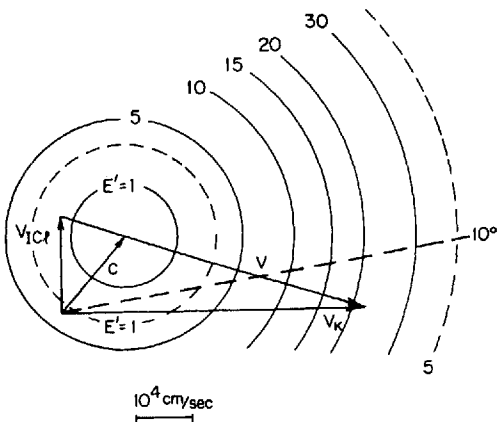
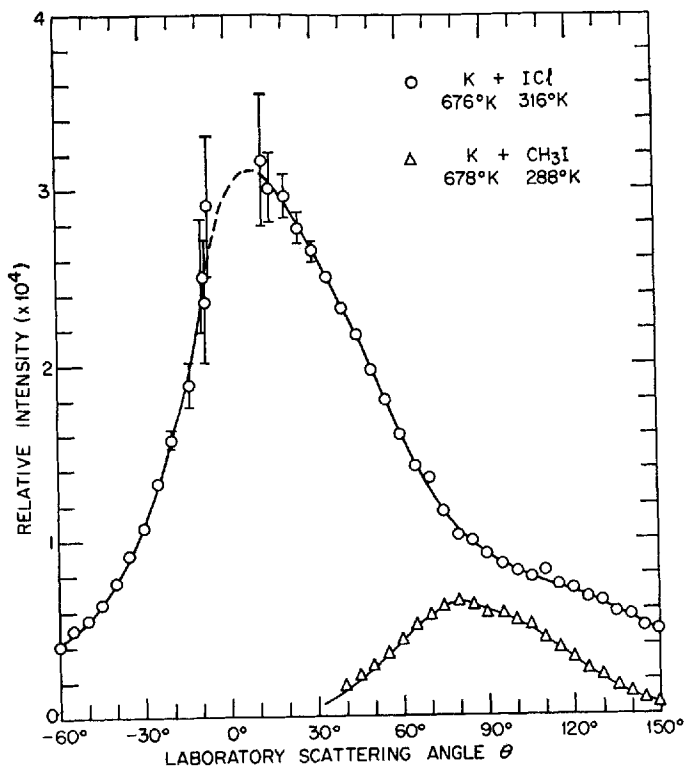


Fig. 6. Comparison of laboratory angular distributions of alkali halide product from the  $K + ICl$  and  $K + CH_3I$  reactions. The kinematic diagram applies to the  $K + ICl$  system; solid circles indicate the recoil energy  $E'$  when KI is the product, dashed circles when KCl is the product.

potential; a very similar distribution is obtained for a Lennard-Jones potential.

The angular distribution of K scattered from  $\text{CH}_3\text{I}$  closely resembles the pattern expected for an Exp-6 or Lennard-Jones potential, and in particular shows at wide angles the bowed shape characteristic for scattering from a repulsive wall. In contrast, the nonreactive scattering

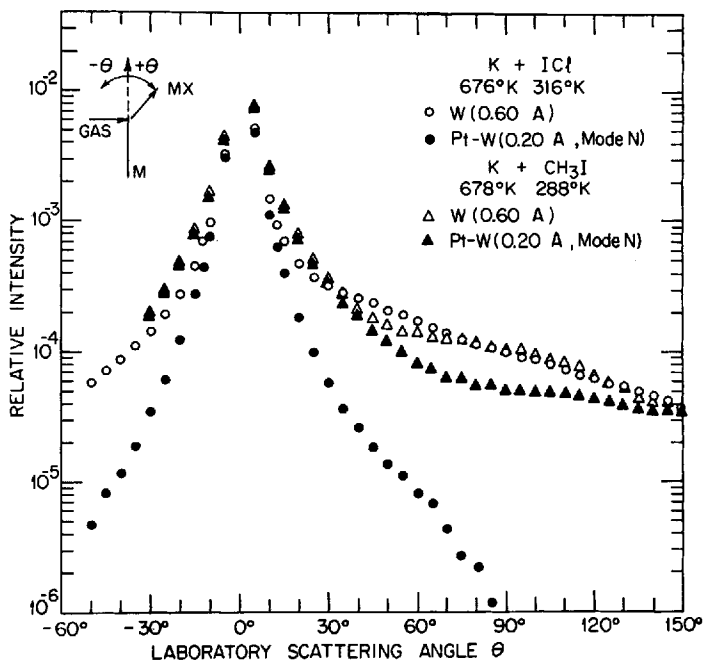


Fig. 7. Comparison of laboratory angular distributions of *total scattering* (sum of M and MX, indicated by ○ or △) and of *nonreactive scattering* (M only, indicated by ● or ▲) for the K + ICl and K +  $\text{CH}_3\text{I}$  systems.

from  $\text{Br}_2$  shows an almost exponential falloff at wide angles. The usual contribution from repulsive core scattering is evidently almost entirely absent. Furthermore, as discussed later, the observed rate of decay of the intensity (by about  $1/e$  in each  $30^\circ$  interval, as indicated by the light dashed curve in Fig. 8) is strong evidence that the only significant contributions to the wide-angle nonreactive scattering come from collisions at large impact parameters which involve "orbiting" outside a

centrifugal barrier. For stripping reactions, collisions at smaller impact parameters apparently lead almost exclusively to reaction, whereas for rebound reactions even close collisions give substantial contributions to the nonreactive scattering.

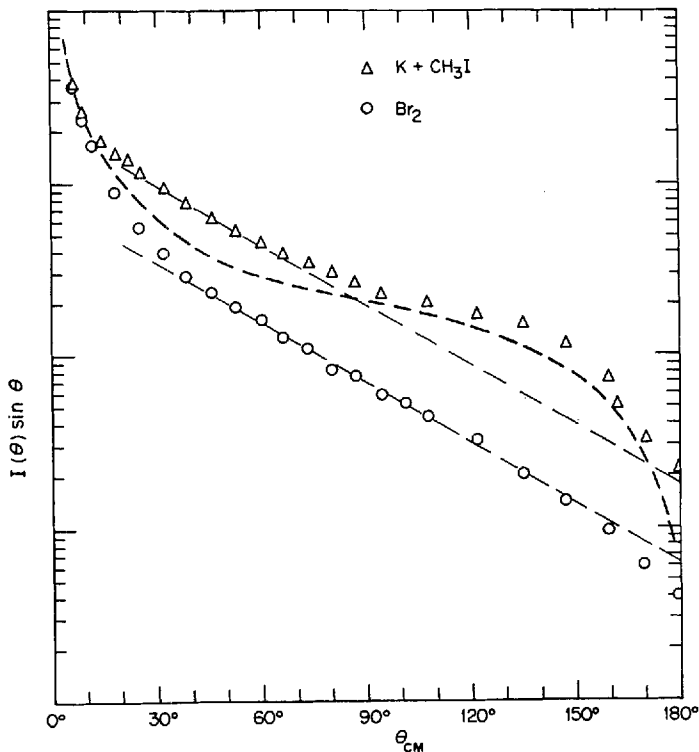


Fig. 8. Comparison of angular distributions (in the center-of-mass system) of K atoms scattered from  $CH_3I$  and from  $Br_2$  without reaction. The heavy dashed curve shows the distribution expected for elastic scattering produced by an Exp-6 potential (with well depth  $\epsilon = 0.5$  kcal/mole and repulsive index  $\alpha = 12$ ); the experimental curves are normalized to this in the small angle region. The light dashed curves are calculated from the orbiting collision model.

Figure 9 shows the CM angular distributions of reactive scattering obtained by using a "fixed-velocity" approximation to carry out the LAB  $\rightarrow$  CM transformation.<sup>65</sup> This is analogous to the treatment applied in Figure 8 to elastic scattering. Only the most probable velocity vectors

in the reactant beams are considered and in addition it is assumed that the recoil energy  $E'$  has a fixed value. The requirement of cylindrical symmetry about the initial relative velocity vector means that for certain portions of the angular distribution different LAB angles should correspond to the same CM angle and intensity, and the value of  $E'$

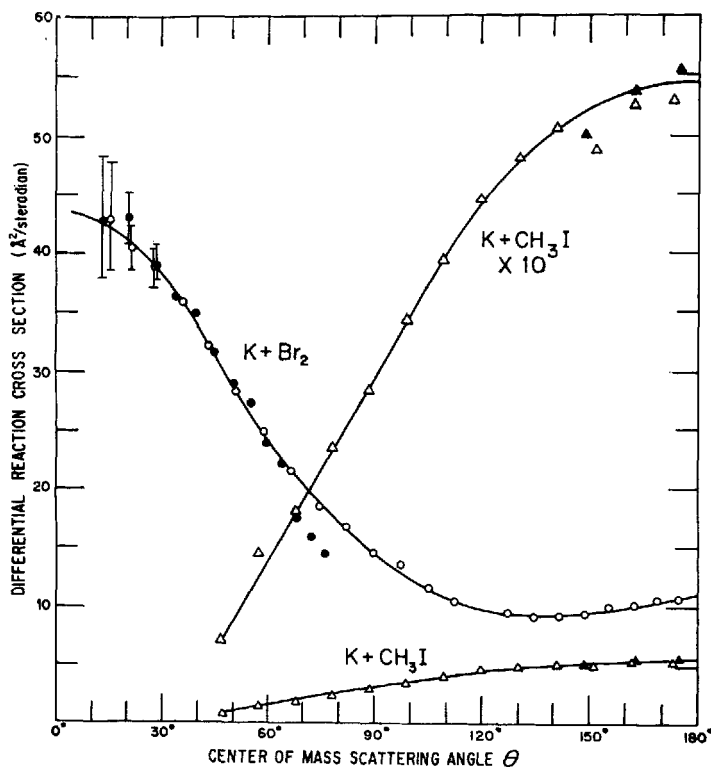


Fig. 9. Comparison of angular distributions (in the center-of-mass system) of alkali halide product from the  $K + CH_3I$  and  $K + Br_2$  reactions, as derived via the fixed velocity approximation.

is adjusted until the results satisfy this requirement as closely as possible. For stripping reactions, for example, the CM results derived from observations at negative LAB angles should match those from part of the range of positive LAB angles (see Figs. 4 and 5). For rebound reactions, the regions of redundant LAB angles are less well separated and accord-

ingly the results are less well defined. This procedure can give only a rough approximation to the actual CM angular distribution but (since it suppresses all the distributions in energy) it probably provides an upper limit estimate for the spread in CM recoil angles. The significance of the value of  $E'$  obtained is less definite; it appears to be higher than the most probable value, as indicated by comparison with other kinematic calculations and the velocity analysis experiment described in Section I-D (see Fig. 13). The analysis also provides an estimate of the total reaction cross section,  $\sigma_r$ . The ratio of  $\sigma_r$  to the total scattering cross section is evaluated by integration of the CM relative intensity distribution; this circumvents the difficulty encountered in the LAB system where often the out-of-plane scattering or other portions of the distributions are out of reach of the detector. In Figure 9, the points derived from the two branches of the LAB distributions are distinguished by open and solid figures. For the  $\text{Br}_2$  reaction the best matching occurs for  $E' = 3.6$  kcal/mole, and  $\sigma_r = 210 \text{ \AA}^2$ ; for  $\text{CH}_3\text{I}$ ,  $E' = 6.3$  kcal/mole, and  $\sigma_r = 30 \text{ \AA}^2$ . The form of the CM product distributions indicated by this approximate analysis agree very nicely with results obtained from the Monte Carlo calculations.<sup>27,32,66</sup>

Outside the series of alkyl iodide reactions there are at present no other definitely established examples of rebound reactions. Many examples of stripping reactions involving polyatomic molecules have been found,<sup>38,40,45,65,67</sup> including  $\text{M} + \text{SiCl}_4$ ,  $\text{PCl}_3$ ,  $\text{PBr}_3$ ,  $\text{CH}_2\text{I}_2$ ,  $\text{SnCl}_4$ ,  $\text{CBr}_4$ , and  $\text{SF}_6$ . In all these the nominal recoil energy  $E' \sim 1$  kcal/mole, and the reaction yield, forward peaking of the alkali halide distribution, and wide-angle falloff of the nonreactive scattering are remarkably similar to those found for the diatomic halogen reactions.

The nature of the transition between the rebound and stripping mechanisms has also been examined.<sup>38</sup> In the early Polanyi sodium flame experiments, several series of related polyhalide molecules were found to show drastic differences in reactivity, and beam studies have been carried out for such a series:  $\text{M} + \text{SiCl}_4$ ,  $\text{CHCl}_3$ ,  $\text{CCl}_4$ ,  $\text{SnCl}_4$ . For  $\text{M} + \text{SiCl}_4$  the reaction yield is too small to be reliably measured, but the scattering provides a reference for comparison with the other members of the series. As in Figure 7, the angular distribution of the *total scattering* for each of the reactive systems is found to be remarkably close to that for the  $\text{SiCl}_4$  standard. Also, again the nominal recoil energy  $E' \sim 1$  kcal/mole for the reactive systems. For  $\text{M} + \text{CHCl}_3$  and  $\text{M} + \text{CCl}_4$ , the yield and other properties are intermediate between those

for the prototype rebound and stripping cases. The laboratory angular distributions of alkali halide appear to be bimodal and correspond to sideways, conical distributions of the recoil velocity vectors. In the wide-angle nonreactive scattering, a substantial contribution with the bowed shape characteristic of repulsive wall scattering appears to be superposed on the exponentially decaying contribution from orbiting collisions. This is illustrated for  $\text{CCl}_4$  in Figure 10 (to be compared with Fig. 8), which includes the results for a drastic stripping case,  $\text{SnCl}_4$ , as well as the nonreactive standard,  $\text{SiCl}_4$ .

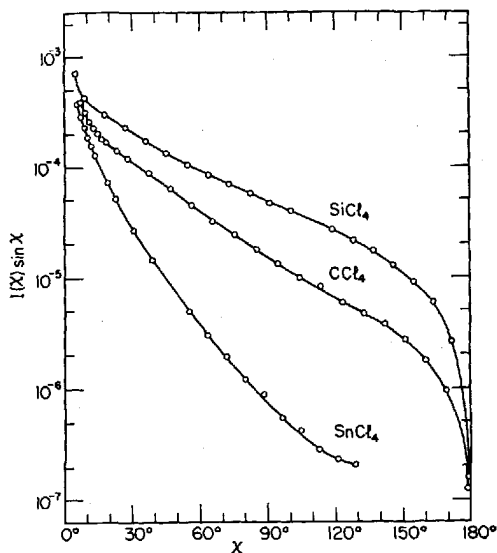


Fig. 10. Comparison of angular distributions (in the center-of-mass system) of Cs atoms scattered from tetrachloride molecules without reaction. (Here the CM scattering angle is denoted by  $\chi$  rather than by  $\theta$  as in Figure 8.)

The results for these polyhalide reactions indicate a strong correlation among the magnitude of the total reaction cross section, the preferred direction of recoil of the products, and the shape of the angular distribution of nonreactive scattering. As the reaction yield increases from the rebound range to the stripping limit, the favored direction for recoil of the alkali halide gradually shifts from backwards to forwards and the falloff in the wide-angle nonreactive scattering of the alkali atoms becomes increasingly pronounced.

### C. Magnetic Deflection Analysis

The inhomogeneous magnet<sup>45</sup> shown in Figure 3*b* is of the traditional design,<sup>53-55</sup> with pole tips which conform to the cylindrical magnetic equipotential surfaces of the field produced by a pair of infinitely long parallel wires carrying equal and opposite currents. The copper tubing wound about the yoke (42 turns of 0.5-cm diameter tubing insulated with Fiberglas sheathing) carries both the energizing current and cooling water. A transistorized power supply is used which provides up to 100 A with less than 0.2% ripple. The magnet barrel is 7.0 cm long and the maximum width of the air gap is 0.32 cm. At an energizing current of 85 A, the induction in the air gap is  $B \approx 11$  kgauss and the transverse gradient is  $\partial B/\partial z \approx 34$  kgauss/cm.

For a given field, the deflection of an uncharged particle is proportional to  $\mu_m/E_t$ , where  $\mu_m$  is the magnetic moment and  $E_t = \frac{1}{2}mv^2$  is the translational kinetic energy. Mass and velocity enter only via  $E_t$ , since the deflection is given by  $\frac{1}{2}at^2$ , with  $a = (\mu_m/m)\partial B/\partial z$  the transverse acceleration and  $t = L/v$  the time of passage through the field. With the field of Figure 3(*b*) operated at 85 A, an atom with  $\mu_m = 1$  Bohr magneton and  $E_t = 1$  kcal/mole is deflected by 0.05 cm in passing through the field ( $L = 7.0$  cm). The deflection at the position of the detector is larger, about 0.11 cm, since the detector is an appreciable distance beyond the magnet ( $D = 4.1$  cm, for the experiments of Fig. 11) and hence the deflection is magnified by a factor  $1 + 2(D/L)$ .

In the experiments of Figure 11 the magnet was used to eliminate most of the background signal due to the paramagnetic alkali atoms and thus permit a direct measurement of the distribution of diamagnetic alkali halide molecules produced by reactive scattering.<sup>31,45</sup> A test of the results which had been obtained from the two-filament subtraction method seemed very desirable because of the great difficulties experienced with "poisoning" in the initial studies of  $K + Br_2$  and other stripping reactions. It appeared that the remarkably large yields and the remarkably similar form of the angular distributions for various reactions indicated by the two-filament results might be spurious.

In the deflection experiments, the magnet and detector assembly are mounted on a common flange and view the scattering chamber through two slits, each 0.01 cm wide; the first slit is 0.5 cm ahead of the magnet and 11.6 cm from the detector; the second slit 6.35 cm ahead of the first and 1.4 cm from the scattering chamber. It is essential that, with

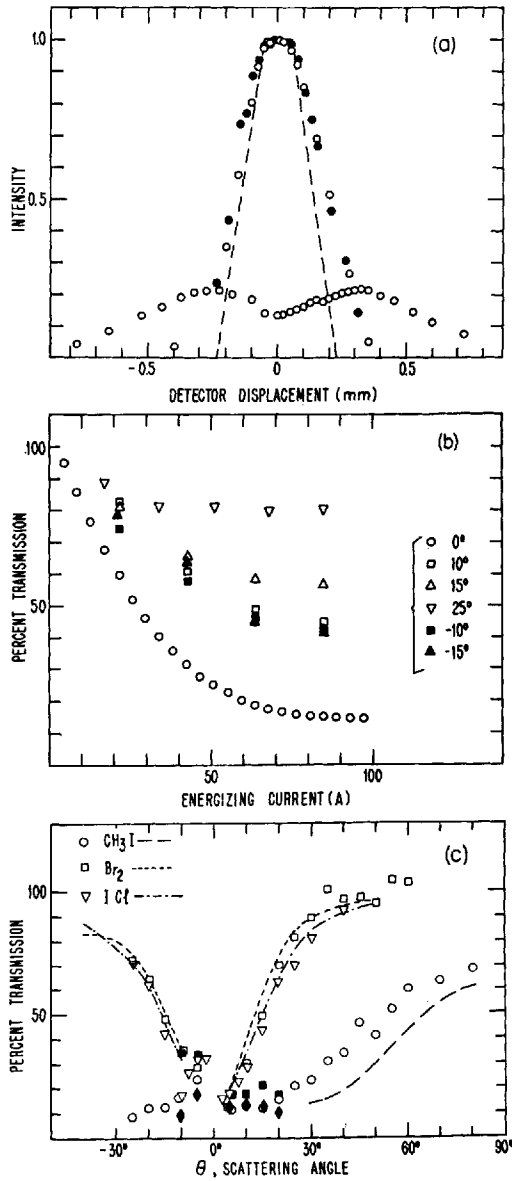


Fig 11. Magnetic deflection analysis: (a) Beam profile (for zero field) calculated from nominal slit geometry (*dashed trapezoid*) compared with profiles observed for parent K beam at  $0^\circ$  (O; unnormalized signal  $5 \times 10^{-10}$  A) and scattered signal at  $25^\circ$  (●; unnormalized signal  $5 \times 10^{-14}$  A). The Stern-Gerlach deflection pattern

the magnet off, the profile of the signal transmitted through the collimating slits and magnet barrel to the detector should remain independent of the observation angle  $\Theta$ , since broadening of the profile by misalignment or background scattering can drastically reduce the effective deflecting power. Figure 11a shows a typical check of this requirement and an example of a deflection pattern. Since relatively wide slits had to be used, about 14% of the parent K beam (including high-velocity atoms and  $\sim 1\%$   $K_2$  molecules) cannot be deflected.

Measurements of the magnetically filtered signal as a function of the magnet current are illustrated in Figure 11b; this demonstrates that for  $K + Br_2$  a large fraction of the scattering at  $\Theta = \pm 10^\circ$  and beyond is due to a diamagnetic product.

In Figure 11c the results for reactions of K with  $CH_3I$ ,  $Br_2$ , and  $ICl$  are compared. Results obtained for the nonreactive system  $K +$  cyclohexane are also shown; as expected, this exhibits the same transmission as the parent K beam. All of the data were obtained with a W filament except for a few points for  $K + Br_2$  (solid squares), which were obtained with a Pt-W filament that had been heated in methane to make it insensitive to  $KBr$ . As the latter points are somewhat higher than those for cyclohexane, it appears that the Pt-W filament still detects some  $KBr$ , but with low efficiency ( $\sim 5\%$ ). The results for the reactive systems are in very good agreement with calculated curves (shown dashed) derived from the previous two-filament measurements. There is clearly a striking difference between the  $CH_3I$  reaction, in which the diamagnetic product appears only at angles beyond  $\Theta \simeq 30^\circ$  and is accompanied by a comparable amount of elastic scattering, and the  $Br_2$  and  $ICl$  reactions, in which the product is a substantial fraction of the signal within  $\Theta < \pm 30^\circ$  and practically 100% of the signal beyond  $\Theta \simeq 30^\circ$ .

Magnetic deflection analysis has subsequently been applied to several other reactions,<sup>45</sup> including some involving nitrogen oxides for which the products could not be detected by the two-filament method.

---

for the parent beam (at a magnet current of 67.6 A) is also shown. (b) Signal reaching detector (at center of beam profile) as a function of the magnet current, for scattering of  $K + Br_2$  at various angles. (c) Comparison of transmitted signal (at a magnet current of 84.4 A) versus laboratory scattering angle for beams of  $CH_3I$  (O, — — —),  $ICl$  ( $\Delta$ , — — —), and cyclohexane ( $\blacklozenge$ ) colliding with the parent K beam. Dashed curves are results predicted from data obtained with the two-filament technique.

#### D. Velocity Analysis of Products

The velocity selector<sup>49</sup> shown in Figure 3a is similar in design to that used by Hostettler and Bernstein<sup>68</sup> and others.<sup>69,70</sup> The rotor, which can be lowered out of the beam path by the gear arrangement, is driven by a hysteresis synchronous motor and a variable-frequency three-phase power supply. Each of the disks has 240 slots 0.080 cm wide, and the intermediate disks are positioned in such a way as to block the transmission of any "overtone" velocities.<sup>68</sup> A band of velocities with an approximately triangular intensity distribution is transmitted; the full width at half-intensity is 4.8% of the nominal transmitted velocity. The effective fractional open time to the incident beam is 0.32. At the highest attainable rotor speed (24,000 rpm) the transmitted velocity is 1200 m/sec.

As yet only a few studies<sup>1,19,29,40,41,44</sup> (a brief review is given in ref. 47) have employed velocity analysis of reaction products. Figure 12 shows results obtained for the  $K + Br_2$  system.<sup>40,41</sup> In these experiments, the parent K beam (at 665°K) had most probable velocity  $\alpha(K) = 530$  m/sec and the  $Br_2$  beam (at 315°K) had  $\alpha(Br_2) = 170$  m/sec. As before, the scattered K signal was detected with a "methanated" Pt-W surface ionization filament and the KBr signal was evaluated by taking the difference between readings on the W filament and the Pt-W filament. As in the experiments with the magnetic or electric analyzers, the apparatus alignment is very important. Only a small part of the zone of intersection of the parent beams is viewed by the detector, which is now 30 cm away and behind two additional collimating slits of width 0.005 cm placed before and after the velocity selector. Thus it is essential to establish that the two detector filaments continue to view the same portion of the scattering zone as the beam source assembly is rotated (see Fig. 1) about the scattering center. For the final alignment, the optimum "undisplaced" position of each filament was determined by scanning the parent K beam profile (at  $\Theta = 0^\circ$ ) with the detector running. Then an auxiliary experiment was carried out on the essentially nonreactive system  $K + SiCl_4$ , to verify that the velocity spectra (at various scattering angles  $\Theta$ ) measured on the two filaments were the same.

In Figure 12 the velocity distributions are given in terms of the "relative number density",  $N(v) = S(v)/v^2$ , obtained (aside from normalization) by dividing the detector signal by the square of the velocity. One of these factors of  $v$  corrects for the transmission of the velocity analyzer, which is proportional to velocity; the other factor of  $v$

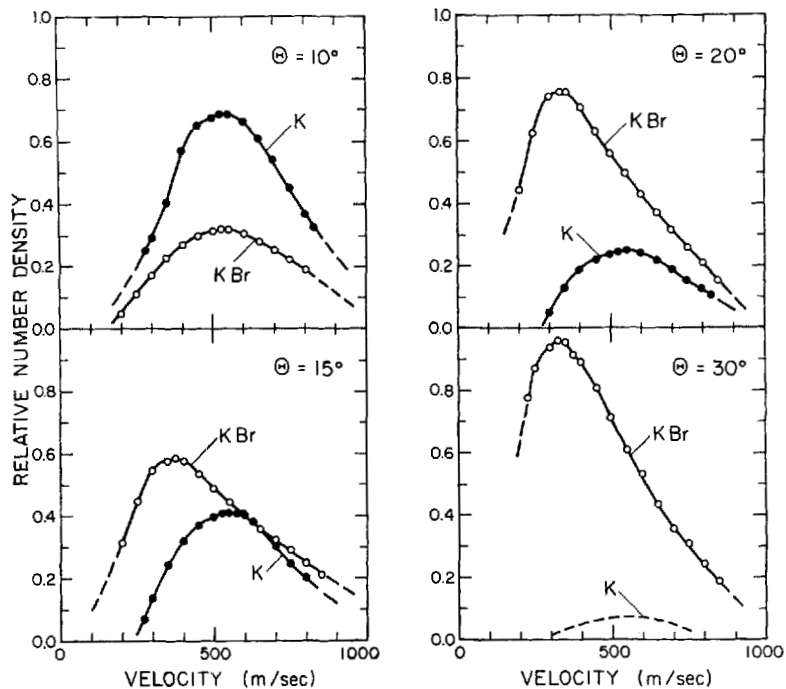


Fig. 12. Velocity analysis of  $K + Br_2$  scattering at various laboratory angles. At each angle, the curves have been normalized so that the sum of the maximum ordinates for  $K$  and  $KBr$  is unity.

converts the flux density (particles/cm<sup>2</sup> sec) measured by the surface ionization detector into a number density (particles/cm<sup>3</sup>). The distributions have been normalized at each angle so that the sum of the maximum ordinates for  $K$  and  $KBr$  is unity.

In agreement with the previous experiments (see Figs. 4 and 11), as  $\Theta$  increases, the intensity of scattered  $K$  falls off much more rapidly than that of  $KBr$ , and at  $\Theta \approx 20^\circ$  and beyond, the reactive scattering is dominant throughout the velocity spectrum. The distribution of scattered  $K$  peaks near 530 m/sec, the most probable velocity in the parent beam, and as  $\Theta$  increases shows only a slight shift to higher velocities (as required by the kinematics of elastic scattering). The  $KBr$  distribution peaks at 510 m/sec for  $\Theta = 10^\circ$  but shifts rapidly to lower velocities as  $\Theta$  increases; the peak appears at about 370, 350 and 310 m/sec for  $\Theta = 15^\circ, 20^\circ,$  and  $30^\circ$ , respectively. Although the velocity

analysis covers just the range 200–900 m/sec, it appears that only a small fraction of the total KBr yield occurs at higher velocities. Differences in conditions (especially the collimation of the parent beams and viewing zone of the detector) preclude a precise comparison with the previous experiments made without velocity analysis. However, the ratio of the integrated intensity in the KBr velocity distribution, including the extrapolated portions indicated in Figure 12, to the total KBr signal observed in the experiments without velocity analysis remains constant (within 10%) as  $\Theta$  is changed.

These results nicely confirm the qualitative kinematic interpretation of the previous angular distribution measurements, and definitely establish that most of the chemical energy released in the  $K + Br_2$  reaction,  $\Delta D_0 \simeq 45$  kcal/mole, must appear in internal excitation rather than in translational motion of the products. In Figure 13 a contour map of the experimental LAB distribution of KBr is compared with the Newton diagram for the most probable velocities in the reactant beams. This indicates that the recoil energy in the CM system which corresponds to the peak in the LAB velocity distribution (shown by the open circles) varies from roughly  $E' = 6$  kcal/mole at  $\Theta = 10^\circ$  to 3 kcal/mole at  $\Theta = 15^\circ$  and 1 kcal/mole at  $\Theta = 30^\circ$ . The recoil energy distribution is quite broad, however, and along the contour with 50% of the peak intensity  $E' \simeq 18$  kcal/mole at  $\Theta = 10^\circ$  and 8 kcal/mole at  $\Theta = 30^\circ$ . A more useful description of the distribution may be given in terms of the cumulative intensity, or fraction of the total yield which appears below a specified recoil energy. For example, integration of the LAB distributions shown in Figure 12 gives

KBr velocity range	< 500	< 700	< 900 m/sec
Approx. $E'$ range	$\gtrsim 5$	$\gtrsim 10$	$\gtrsim 20$ kcal/mole
Cumulative yield			
at $\Theta = 10^\circ$	40%	79%	95%
at $\Theta = 20^\circ$	61%	86%	94%

To pursue further the analysis of these results, it is necessary to examine the LAB  $\rightarrow$  CM transformation in detail.<sup>40,41</sup> This will not be considered here except to note that the LAB intensity distributions used in constructing Figure 13 must be multiplied by a Jacobian factor to adjust to the CM velocity scale. This factor shifts the peak of the distributions outwards, and thereby moves the 100% contour further from the initial relative velocity vector  $V$  than it appears to be in Figure 13. There remains considerable uncertainty in the quantitative kinematic analysis because of the velocity distributions in the parent beams and

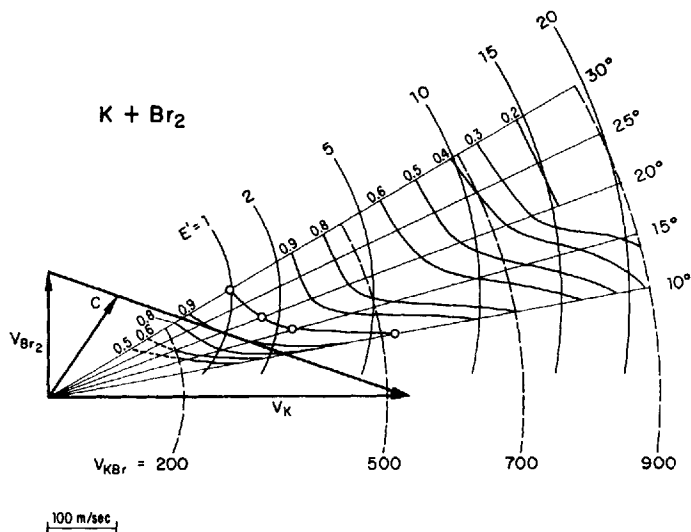


Fig. 13. Contour map indicating kinematic analysis of observed laboratory velocity distribution of KBr from  $K + Br_2$  reaction. Solid circles show loci of  $u_{KBr}$  recoil vectors corresponding to various values of final relative energy  $E'$ ; dashed circles show loci of  $v_{KBr}$  vectors corresponding to various laboratory velocities. Contours denote the percentage of maximum intensity at each laboratory angle; thus they do not indicate the angular variation of intensity but only the variation along the radius corresponding to the fixed value of  $\Theta$ .

the inherent difficulty of evaluating separately the dependence on the recoil angle and energy.

The  $K + Br_2$  reaction has been studied subsequently by the Wisconsin group,<sup>44</sup> with both velocity selection of the parent K beam and velocity analysis of the scattered K and KBr. Measurements were made at  $\Theta = 20^\circ$  with  $v_K = 549, 732,$  and  $915$  m/sec and at  $\Theta = 15^\circ$  and  $10^\circ$  with  $v_K = 549$  m/sec. The KBr distributions obtained turn out to be remarkably similar in position and shape to those of Figure 12; selection and variation of the K velocity appears to have practically no effect on the KBr distribution! This striking property and the qualitative shape of the KBr distributions both find a ready explanation<sup>40,41</sup> in terms of the "electron jump" mechanism discussed in Section II.

### E. Electric Deflection Analysis

Inhomogeneous electric deflecting fields have long been used in beam experiments designed to measure atomic polarizabilities or electric

dipole moments and also for selection of rotational states of polar molecules in electric resonance spectroscopy.<sup>53-55</sup> In scattering experiments, such fields offer a means to examine orientational effects,<sup>71,72</sup> inelastic rotational energy transfer,<sup>73</sup> and the distribution of angular momentum in reaction products.<sup>45,46</sup> The partitioning of angular momentum is of great interest for the theory of reaction dynamics.<sup>10,13,15,27,32,47,52</sup> It is intimately connected with the molecular mechanism of the reaction, since mass, velocity, and position all enter into the definition of angular momentum. Spectroscopic experiments have indicated the presence of high rotational excitation in some reactions but very little is known beyond this because rotational energy is relatively easily degraded by collisions.<sup>74</sup> Thus, beam experiments may make a particularly valuable contribution here.

Conservation of angular momentum provides that

$$\mathbf{L}' + \mathbf{J}' = \mathbf{L} + \mathbf{J} \quad (3)$$

where  $\mathbf{L}$  and  $\mathbf{L}'$  denote the initial and final orbital angular momenta associated with the relative motion of the collision partners and  $\mathbf{J}$  and  $\mathbf{J}'$  denote the rotational momenta of the reactants and products. Classically,

$$L = \mu V b \quad \text{and} \quad L' = \mu' V' b' \quad (4)$$

in terms of the reduced masses, relative velocities, and impact parameters of the reactants and products, respectively. For an  $A + BC \rightarrow AB + C$  reaction,

$$W_{\text{rot}} = J^2/2I \quad \text{and} \quad W'_{\text{rot}} = J'^2/2I', \quad (5)$$

in terms of the initial and final rotational excitation and the moments of inertia of BC and AB, respectively. As indicated in Figure 14a, the  $\mathbf{L}$  vectors are perpendicular to the initial relative velocity  $\mathbf{V}$ , with all azimuthal orientations of  $\mathbf{L}$  about  $\mathbf{V}$  equally likely, whereas the initial  $\mathbf{J}$  vectors are randomly oriented. The total angular momentum  $\mathbf{L} + \mathbf{J}$  supplied by the reactants may be estimated roughly, as the thermal distributions of  $\mathbf{V}$  and  $\mathbf{J}$  are known and the range of impact parameters involved in the reaction probably does not extend much beyond  $b^* \sim (\sigma_r/\pi)^{1/2}$ , where  $\sigma_r$  is the total reaction cross section. For the alkali atom reactions this typically gives  $L \gg J$ , with  $L^*$  ranging from roughly 100 to 250  $\hbar$ .

The partitioning of the angular momentum between  $\mathbf{L}'$  and  $\mathbf{J}'$  in the

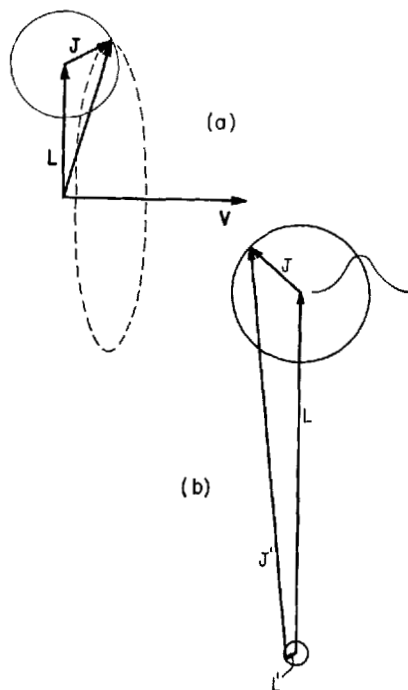
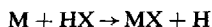


Fig. 14. Orientation of asymptotic angular momentum vectors: (a) In initial state of the collision the orbital angular momentum  $L$  is perpendicular to the relative velocity  $V$ , with all azimuthal orientations equally likely; the direction of the rotational angular momentum  $J$  of the reactants is uniformly distributed. (b) Example for which rotation of products must be polarized, with  $J'$  confined to directions nearly parallel to  $L$  and hence perpendicular to the initial relative velocity vector.

products is often only weakly constrained by the conservation laws. For example, if  $L'$  and  $J'$  are oppositely directed, Eq. (3) allows both to have much larger magnitude than  $|L + J|$ . Energy conservation limits the magnitude of  $J'$  according to Eqs. (2) and (5). However, for strongly exothermic reactions which produce molecules with large moments of inertia, this limit is rather weak; for example, if  $J' \sim 300 \hbar$ , the rotational excitation is  $W'_{rot} \sim 33$  kcal/mole for a KCl molecule, 21 kcal/mole for KBr, and only 9 kcal/mole for CsI. The accessible range of  $L'$  is linked by Eq. (4) to the final relative translational momentum and to the exit impact parameter. Also the centrifugal energy associated with the products,  $L'^2/2\mu'R'^2$ , must not exceed the available

energy (at a radius  $R'$  where  $L'$  and  $J'$  reach their asymptotic values). Again, for a strongly exothermic reaction, a wide range in  $\mu'V'$  and centrifugal energy is usually compatible with energy conservation. The impact parameter  $b'$  is expected to be limited by the range of the forces and probably cannot become much larger than a typical bond length, but this usually allows a quite generous range for  $L'$ . For example, in the  $K + Br_2$  reaction, if  $b' \sim 3\text{\AA}$ , then  $L' \sim 100 \hbar$  for  $E' = 1$  kcal/mole and  $\sim 300 \hbar$  for  $E' = 10$  kcal/mole.

A situation in which the partitioning of angular momentum is tightly constrained by the conservation laws occurs in the reactions



Here it is expected<sup>10,13,15</sup> that most of the available angular momentum will appear in rotation of the MX molecule. On the reactant side, orbital angular momentum is dominant almost everywhere (except where  $b$  or  $V$  is very small), since the small moment of inertia of HX ensures that  $J$  is very small (only  $\sim 3 \hbar$  for HBr at the maximum of the thermal distribution for 300°K). On the product side, however, the orbital angular momentum is likely to be almost negligible; that is,  $\mu'V'b'$  should have a much smaller range than  $\mu Vb$ , since the reduced mass of the products (approximately just the mass of H) is far smaller than that of the reactants (26 times smaller for the  $K + HBr$  reaction, 50 for  $Cs + HBr$ ). Because the reaction is only slightly exothermic,  $V'$  cannot become large enough to offset more than a fraction of the mass ratio; and the exit impact parameter  $b'$  would have to be unreasonably large to make the range of  $L'$  comparable to that of  $L$  (for example,  $b' \sim 15 \text{\AA}$  at  $E' \sim 2$  kcal/mole to make  $L' \sim 100 \hbar$ ). Therefore, since  $L \gg J$  and  $L \gg L'$ , most of the initial orbital angular momentum must appear in product rotation, and  $L \approx J'$ .

The Monte Carlo studies of reaction dynamics<sup>18,27,32</sup> indicate that the condition  $L \approx J'$  may also hold for a large class of reactions for which it is not required by the conservation laws. This occurs also for some of the reaction models discussed in Section II. The  $L \approx J'$  situation has two interesting consequences for an electric deflection experiment.<sup>10,15,45</sup> First, as illustrated in Figure 14*b*, the rotation of MX should be strongly polarized, with  $J'$  aligned nearly perpendicular to the direction of the initial relative velocity vector. The predicted alignment for many reactions is much stronger than could be achieved with an external field and should have a pronounced effect on the electric

deflection patterns. Thus it will be possible to establish experimentally whether the condition  $L \approx J'$  actually occurs. Second, when this does occur, a measurement of the distribution of the rotational momentum of MX will give information about the distribution of initial orbital angular momentum in those collisions which lead to reaction. From Eq. (4), this is equivalent to determining the reaction probability as a function of the initial impact parameter,  $P(b)$ , since the velocity dependence can be determined in separate experiments. The  $P(b)$  function is basic for all theoretical calculations but the only other means of estimating  $P(b)$  from scattering experiments is quite indirect and has to rely on the use of an optical potential model.<sup>13,16,43</sup>

The electric deflection experiment is essentially similar to magnetic deflection. However, the Stark effect of a polar molecule is much more complicated than the Zeeman effect of a paramagnetic atom, and the strength of the Stark effect varies drastically for the myriad rotational states that differ in magnitude and orientation of the angular momentum.<sup>53-55</sup> For heavy molecules such as alkali halides (unless the rotational excitation is extremely low) the effective dipole moment component in the field direction thus has a broad, practically continuous spectrum of values. Despite this, the main features of the rotational distribution can be readily characterized from the electric deflection patterns (if the distribution of transit times through the field is known from velocity analysis). The property most easily determined is the mean rotational energy. This may be evaluated by simply measuring the total fraction of the beam which is deflected and its variation with field strength, since rotation produces a "gyroscopic" quenching of the Stark effect. Information about the form of the rotational energy distribution and the spatial orientation of the angular momentum vectors can be obtained from the shape of the deflection pattern and its variation with the direction of the deflecting field.

The experiments carried out thus far<sup>45,46</sup> have used the apparatus of Figure 3c, which is well suited for measurements of the total deflection but not for measurements of the true shape of the deflection pattern. Since the onset of the field region is abrupt and the direction of the lines of force varies over a wide range, it is likely that any possible polarization would be blurred out by reorientation of the angular momentum within the field.<sup>54</sup> Also, since velocity selection was not used in these experiments, there is a broad spread in the direction of the axis of polarization (i.e., the initial relative velocity vector). Buffer

fields which will preserve the angular momentum quantization<sup>54</sup> must be installed before reliable measurements of the shape of the deflection pattern can be made. Thus, we shall consider here only the results derived from the total deflection measurements.

The experimental configuration is closely analogous to that used for magnetic deflection. The electric field and detector assembly are mounted on a common flange and view the scattering center through two slits, each 0.01 cm wide; the first slit is 1.6 cm ahead of the field and 29.8 cm from the detector; the second is 7.6 cm ahead of the first and 3.9 cm from the scattering center. The electrode configuration, as shown in Figure 3c, again has the "two-wire" form, which produces an electric field conjugate to that from two parallel line charges of opposite sign.<sup>53,54</sup> The electrodes are 15.2 cm long. The radius of the concave electrode is 0.396 cm and the radius of the convex electrode and the maximum width of the air gap are both 0.317 cm. The concave electrode is grounded and the convex electrode is charged by a transformer capable of supplying up to 50 kV at a current of 5 mA with less than 2% ripple. To minimize sparking, the electrodes are made of polished stainless steel and the insulators are quartz. In practice the sparking voltage is determined by surface contamination; in a good vacuum (no parent beams, background pressure  $\approx 10^{-7}$  mm Hg) it is about 40 kV after the electrodes have been carefully cleaned and "purged" for several hours by repeatedly turning up the voltage to "spark away" specks of dirt, whereas with the parent beams present it drops to between 20 and 30 kV. The end plates shown in Figure 3c are attached to the grounded electrode when the apparatus is assembled; these carry some of the slits and provide part of the electrical shielding between the detector and field. The entire assembly (field, slits, detector, etc.) is enclosed in a 10-cm diameter brass tube attached to the main beam apparatus by a rotatable vacuum seal, and the fan shown in Figure 3c allows the electrical contact to be maintained as the orientation of the field is adjusted.

Auxiliary runs with thermal beams were carried out regularly to test the apparatus alignment and to provide a direct calibration of the deflecting power of the field. Calculations from Stark effect theory<sup>45</sup> were found to give excellent agreement with the deflection patterns observed in these runs if it was assumed that the beam passed 0.17 cm from the convex electrode (this is within the uncertainty in the position estimated from the nominal slit geometry). At this position the field

strength and transverse gradient calculated from the field geometry are  $\mathcal{E} = 2.97 V_0$  (kV/cm) and  $\partial\mathcal{E}/\partial z = -8.63 V_0$  (kV/cm<sup>2</sup>), where  $V_0$  (kV) is the applied potential. With this field operated at  $V_0 = 30$  kV, a neutral particle with an effective dipole moment component of only 0.01 Debye and translational energy  $E_t = 1$  kcal/mole will undergo a deflection of about 0.02 cm at the detector. An MX molecule has a permanent dipole moment of  $\sim 10$  D and the magnitude of the effective moment (averaged over isotropic rotational orientations) remains larger than  $\sim 0.01$  D until the rotational energy  $E_r$  exceeds  $\sim 20$  kcal/mole (e.g., corresponding to  $J' \simeq 300 \hbar$  for KBr).

Figure 15a shows typical beam profiles and deflection patterns observed for KBr from reactive scattering of  $\text{K} + \text{Br}_2$  and for thermal Cs and CsCl calibration beams. The reproducibility of the apparatus alignment is illustrated by the close agreement (for runs made three months apart) with the zero-field profile calculated from the nominal slit geometry (dashed trapezoid). The deflection pattern for the Cs beam is shifted bodily towards the high-field region by the polarizability interaction (at 30 kV the induced dipole is about 0.015 D). The patterns for the reactively scattered KBr (at a laboratory angle  $\Theta = 40^\circ$  from the K beam) and the CsCl calibrating beam spread to both high and low field since the dipole moment has a range of orientations with respect to the field direction. The deflection pattern for the KBr product is seen to be very similar to that for a thermal beam. This is observed also for several other reactions which were studied, including the  $\text{Cs} + \text{HBr}$  reaction. Taken at face value, the shape of the pattern thus would correspond to an isotropic distribution of  $J'$  vectors. As already discussed, this may be a spurious result caused by experimental blurring of a polarized orientation, but the width of the deflection pattern remains a significant measure of the average rotational excitation.

Figure 15b shows measurements of the total deflection, in terms of the signal reaching the detector (at the center of the zero-field beam profile) as a function of the electrode voltage, for reactively scattered KBr from  $\text{K} + \text{Br}_2$  and CsBr from  $\text{Cs} + \text{HBr}$ . Also shown are results for elastic scattering of K from cyclohexane (at  $\Theta = 30^\circ$ , open diamonds) and for thermal beams of K, Cs, and CsCl. The reactive scattering curves have been corrected for the contributions from deflection of atoms elastically scattered at the same angle.

The results clearly demonstrate that in these reactions the mean rotational excitation of the newly formed products is comparable to the

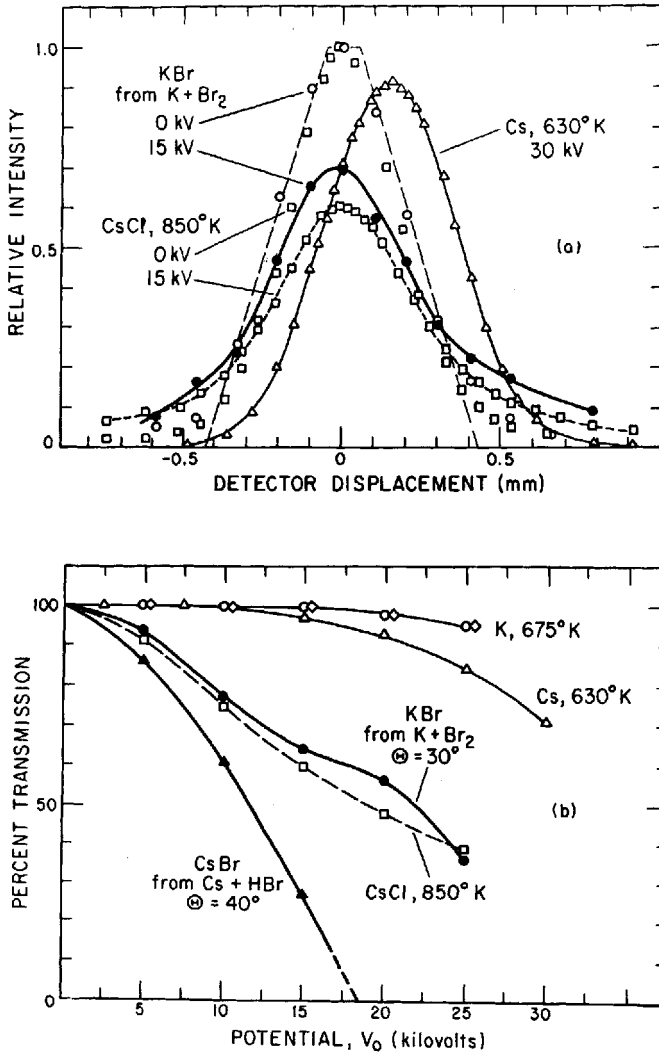


Fig. 15. Electric deflection analysis: (a) deflection patterns; (b) variation of transmission with electrode voltage.

thermal energy. As illustrated in Figure 16, the total deflection depends primarily on the ratio  $\mu\mathcal{E}/\langle\bar{E}\rangle$ , where  $\mu\mathcal{E}$  is the Stark effect perturbation energy and  $\bar{E} = (E_t E_r)^{1/2}$  is the geometric mean of the translational and rotational energy; in the accessible range the total deflection is insensitive both to the form of the distribution in  $E_r$ , and to the orientation of the angular momentum vectors. A thermal translational distribution is assumed (temperature  $T_t$ ). For K + Br<sub>2</sub> the direct measurements<sup>41</sup> show this is a good approximation (with  $T_t \approx 755^\circ\text{K}$  at  $\Theta = 30^\circ$ ). For Cs + HBr, kinematics requires the CsBr to come off very near the center of mass; thus the velocity distribution is readily calculated and again it is approximately thermal (with  $T_t \approx 375^\circ\text{K}$  at  $\Theta = 40^\circ$ ). For the

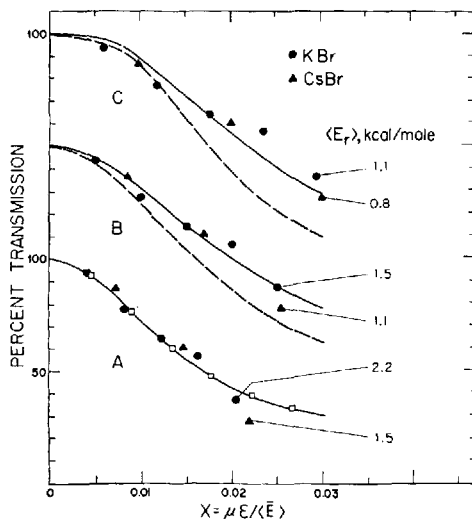


Fig. 16. Transmission functions calculated for various rotational energy distributions compared with experimental results.

rotational distribution, case *A* is a thermal distribution (temperature  $T_r$ ), *B* is a constant up to a cutoff (denoted by  $E_B$ ), *C* is a delta function (located at  $E_C$ ); the first moments are related by

$$\langle E_r \rangle = kT_r = \frac{1}{2}E_B = E_C$$

The solid curves refer to isotropic orientation, dashed to polarization perpendicular to the field direction. The data have been fitted to the calculated curves by adjusting the value of  $\langle E_r \rangle = \langle \bar{E} \rangle^2 / kT_t$ ; for each

case the isotropic orientation was used, since, as shown in Figure 15a, this corresponds closely to the measured deflection patterns.

As noted above, the total angular momentum available to the products may be roughly estimated from the magnitude of the observed reaction cross sections. For  $\text{Cs} + \text{HBr}$  ( $\sigma_r \approx 140 \text{ \AA}^2$ ), essentially all of it ( $175 \hbar$ , estimated from case *B*, polarized) appears to go into rotation of  $\text{CsBr}$  as predicted from analysis of the kinematic restrictions on this reaction.<sup>10,13,15</sup> For  $\text{K} + \text{Br}_2$  ( $\sigma_r \approx 210 \text{ \AA}^2$ , corresponding to at least  $250 \hbar$  available), kinematic restrictions are insignificant and the deflection experiments indicate the rotational momentum of  $\text{KBr}$  is appreciably smaller (case *B*, polarized gives the maximum as  $135 \hbar$ ) so that a substantial fraction must appear in the orbital angular momentum associated with the relative motion of  $\text{KBr}$  and  $\text{Br}$ .

Electric deflection measurements have been carried out also<sup>45</sup> for reactions of alkali metals with  $\text{ICl}$ ,  $\text{PBr}_3$ ,  $\text{SnCl}_4$ , and  $\text{SF}_6$ . The values found for  $\langle \bar{E} \rangle$  range from 1 to 3.5 kcal/mole. Although the evaluation of  $\langle E_r \rangle$  must await completion of velocity analysis experiments, these results show that in all of these reactions the exothermicity must appear mostly in vibrational excitation (or possibly electronic excitation) of the products.

## F. Summary and Discussion

Table I and the bibliography<sup>1-52</sup> are intended to provide a complete list of molecular beam studies of reactive scattering and theoretical discussions of the results. References to the earliest proposals and inconclusive experiments are omitted since these can be found in other reviews.<sup>3,47,53</sup> Thus the bibliography goes back only ten years<sup>1,2</sup> and over two-thirds of the entries have appeared within the past two years. Also, studies of the elastic scattering of reactive molecules have been extensively reviewed elsewhere.<sup>16,21,43</sup> References to this work are not included in Table I (except when carried out concurrently with reactive scattering experiments) but are included in the bibliography. The same holds for a few preliminary studies of reactive scattering for which the present data are very incomplete or appear inconsistent with kinematic requirements.

The broad, qualitative features which have appeared again and again in the work of Table I may be summarized as:

1. Most of the chemical energy released appears as internal excitation of the products rather than as relative translational kinetic energy.

TABLE I  
 Reactions Studied in Molecular Beams<sup>a</sup>

Reaction	$\Delta D_0$ , kcal/mole	Refs.
$K + HBr \rightarrow KBr + H$	3.8	2,3,5,6,8,13,16,21,23,29,36, 43,45,46
$HI \rightarrow KI + H$	5.6	25,35,43
$M + RI \rightarrow MI + R$		7,10,14,15,16,21,24,
M = Na, K, Rb, Cs		26,27,31,32,38,47,48,
R = CH <sub>3</sub> , C <sub>2</sub> H <sub>5</sub> , ... , C <sub>5</sub> H <sub>11</sub>	23-33	49,50
R = CH <sub>2</sub> : CHCH <sub>2</sub>	40	
$M + Br_2 \rightarrow MBr + Br$	44.8	28,31,38,39,40,41,42,44,45, 46,47,66
I <sub>2</sub> → MI + I	40.4	38,39,42,47
ICl → MI + Cl	26.4	31,39,47,49
or → MCl + I	51.0	
IBr → MI + Br	34.1	39,47,49
or → MBr + I	48.3	
$M + SCl_2 \rightarrow MCl + SCl$	~40	40
$M + PCl_3 \rightarrow MCl + PCl_2$	~22	38
$PBr_3 \rightarrow MBr + PBr_2$	~27	
$M + CH_2I_2 \rightarrow MI + CH_2I$	(30)	65
$M + CHCl_3 \rightarrow MCl + CHCl_2$	~32	38
$CHBr_3 \rightarrow MBr + CHBr_2$	~40	
$M + SnCl_4 \rightarrow MCl + SnCl_3$	~24	38,45
$CCl_4 \rightarrow MCl + CCl_3$	32	1,38,45,47
$CBr_4 \rightarrow MBr + CBr_3$	~40	38,67
$M + SF_6 \rightarrow MF + SF_5$	(50)	45
or → MSF <sub>5</sub> + F	(?)	
$M + CF_3I \rightarrow MI + CF_3$	(23)	75
$M + NO_2 \rightarrow MO + NO$	(30)	45
+ CH <sub>3</sub> NO <sub>2</sub> → MNO <sub>2</sub> + CH <sub>3</sub>	(20)	45

<sup>a</sup> The italicized references give experimental results, others give discussion or interpretation. The quantity  $\Delta D_0$  is the difference in dissociation energy of the M—X bond (from ref. 77) and the reactant R—X bond (from ref. 76), measured from the zero-point vibrational level. The values given refer to reactions with potassium; for a given halogen, the  $\Delta D_0$  values would be almost the same for reactions with rubidium, about 3–4 kcal/mole less for reactions with sodium, and about 5 kcal/mole larger for reactions with cesium. The listed values are all uncertain by about 1–2 kcal/mole due to uncertainty in the M—X bond strengths. For the cases indicated with an approximation mark there is a further uncertainty of perhaps 5 kcal/mole or more because only an average value of the R—X bond strength derived from the heat of atomization of the compound is available. Values given in parenthesis are much more uncertain, and in most cases are simply guesswork.

2. The angular distribution of products (in the CM system) is usually quite anisotropic. With respect to the incoming M atoms, most of the MX molecules recoil *backwards* in the rebound reactions (e.g., alkyl iodide reactions), *forwards* in the stripping reactions (e.g., diatomic halogens,  $\text{SCl}_2$ ,  $\text{PCl}_3$ ,  $\text{SnCl}_4$ ), and *sideways* for intermediate reactions (e.g.,  $\text{CCl}_4$ ,  $\text{CHCl}_3$ ,  $\text{CF}_3\text{I}$ ).

3. The preferred direction of recoil of the products is strongly correlated with the magnitude of the total reaction cross section,  $\sigma_r$ , which varies from  $\approx 10 \text{ \AA}^2$  for rebound reactions to  $\approx 100 \text{ \AA}^2$  for stripping reactions.

4. The shape of the angular distribution of elastic scattering (in the CM system) also is correlated with  $\sigma_r$ ; for rebound reactions, it is similar to that of comparable nonreactive molecules, whereas for stripping reactions it falls off very rapidly at wide angles.

5. Regardless of the size of  $\sigma_r$ , the angular distribution of the total scattering (sum of elastically scattered M and reactively scattered MX) is similar to that for nonreactive molecules of similar size and structure.

More detailed properties, thus far studied for only a few reactions, include:

6. The shape of the angular distributions (CM system) of both the reactive and nonreactive scattering is almost identical for various alkali metals ( $M = \text{K}, \text{Rb}, \text{Cs}$ ) but may differ appreciably for different reactant molecules (e.g., for  $\text{Br}_2$  and  $\text{I}_2$ ).

7. Variation of the K velocity has very little effect on the velocity of the KBr formed in the  $\text{K} + \text{Br}_2$  reaction.

8. The mean rotational excitation of the products is comparable to their mean translational or thermal energy. In some cases, a large fraction of the initial angular momentum may be taken up in the orbital motion of the products (e.g., the  $\text{K} + \text{Br}_2$  reaction); in others essentially all of it may go into rotational excitation (e.g., the  $\text{Cs} + \text{HBr}$  reaction).

We will consider in turn the interpretation to be attached to each of these properties. As a matter of doctrine, we wish to emphasize the three natural and distinct stages in analysis of chemical scattering studies: kinematic reduction of the data; stochastic comparison with theoretical models based on assumed force fields; and inference or speculation about the chemical basis of the forces. Passage between these stages should be made cautiously! Hence, in reviewing the experimental results we have restricted attention to the kinematic stage, and in order to indicate the proper distance between the experiments and

the final stage we have removed discussion of the chemical implications to Section II. In the stochastic comparison with theoretical models, the Monte Carlo calculations provide the surest guide. Several reviews are available,<sup>26,27,32,74</sup> although the experiments have since pulled ahead of the computers. Here we shall briefly discuss qualitative arguments which are in part supported or suggested by the Monte Carlo results. These interpretations are strictly heuristic.

**Energy Disposal.** The partitioning of the reaction exothermicity between the internal and external degrees of freedom available in the products (property *I*) had received a great deal of attention long before the molecular beam studies. The early Polanyi flame experiments<sup>78-84</sup> showed that many reactions of alkali metals with halogen compounds produced MX with internal excitation sufficient to excite resonance lines of the M atoms in subsequent collisions. However, the observed quantum yields of chemiluminescence were large for only two or three of the reactions; thus, only for these reactions is it possible to conclude that a large fraction of the MX produced must carry high internal excitation. The example universally quoted is the X + Na<sub>2</sub> reaction<sup>78,79</sup> (for which  $\Delta D_0 = 80, 69, 55$  kcal/mole for X = Cl, Br, I as compared with 48 kcal/mole required to excite the Na D lines). This occurs as a secondary step following the Na + X<sub>2</sub> reaction, for which the flame studies give no information concerning the internal excitation since the exothermicity is not large enough to give NaX that could excite the Na D lines. Surprisingly, similar studies<sup>80</sup> of the K + X<sub>2</sub> systems seem to have been almost universally overlooked in texts and reviews. Here the exothermicity ( $\Delta D_0 = 43, 45, 40$  kcal/mole for X = Cl, Br, I) exceeds the excitation energy of the K D lines (37 kcal/mole) and intense chemiluminescence due to the primary reaction was indeed observed. This was separated from a weaker contribution due to the secondary X + K<sub>2</sub> reaction by heating to temperatures sufficient to dissociate most of the K<sub>2</sub> molecules.

In recent years, vibrationally excited product molecules have been directly observed in many spectroscopic experiments. Extensive reviews of this work are available.<sup>74,85-89</sup> Again, however, it should be emphasized that as yet there are only a few studies from which it is possible to establish the order of magnitude of the relative yield of excited and unexcited products or to infer the initial distribution of vibrational excitation before degradation by collisions. For several hydrogen atom reactions, including reactions with Cl<sub>2</sub>, ClNO, and NO<sub>2</sub>, the spectroscopic

observations have shown that the products are formed predominantly in the ground vibrational state.<sup>74,90,91</sup>

The molecular beam and spectroscopic experiments are complementary, since the beam studies can directly determine only the initial translational and rotational energy distributions and the spectroscopic experiments only the steady-state vibrational and electronic excitation. We have recently given a more detailed review<sup>47</sup> of the beam results on energy partitioning. Here we shall only note that although the beam results for the  $M + \text{Br}_2$  and  $M + \text{I}_2$  reactions leave open the question whether the internal excitation is partly present as electronic excitation of the metastable  $^2P_{1/2}$  states of the halogen atoms (10.5 and 21.7 kcal/mole above the ground states for Br and I, respectively), the diffusion flame experiments<sup>80</sup> offer evidence against this.

Early qualitative discussions<sup>78,81</sup> suggested a simple relation between the partitioning of the reaction exothermicity and the form of the potential energy surface. This applies to an  $A + BC \rightarrow AB + C$  reaction without appreciable activation energy. If the surface is of the *attractive* or *early downhill* type, in which most of the exothermicity is released as the reactants approach rather than as the products separate, strong vibrational excitation of the newly formed AB bond is expected, whereas for a *repulsive* or *late downhill* surface most of the exothermicity is expected to appear in translational recoil of AB and C. The energy partitioning has been thoroughly examined in the Monte Carlo studies and found to obey this criterion although in extreme cases other features of the surface have some effect also.<sup>27,33,74,89</sup> Several instructive qualitative discussions of the operation of this criterion have also been given.<sup>89,92-94</sup>

Thus the reactions of alkali atoms and of hydrogen atoms with halogens appear to be prototype examples of the attractive and repulsive type, respectively. Chemical intuition, which always works best after the facts are established, hastens to suggest that these examples probably represent the limiting cases. The strongly attractive or early downhill character of the alkali reactions may be attributed to the transition from covalent ( $X_2$ ) to ionic ( $M^+X^-$ ) bonding (as discussed in Section II), the late downhill character of the hydrogen reactions to the small size and resistance to polarization of the atom, which delays the onset of chemical interaction.

**Angular Distribution of Products.** The marked forward-backward asymmetry observed in the angular distributions of alkali halides in both

the rebound and stripping reactions (property 2, cf. Fig. 9) indicates that the products *remember* the direction of the initial relative velocity vector  $\mathbf{V}$ . These reactions hence proceed mainly via a *direct* or *impulsive* mechanism, rather than via a collision complex whose decomposition could be treated as independent of its manner of formation.<sup>10,15,47</sup> The asymmetry implies that the collision complex usually decomposes before it can rotate through a half-turn. Since most of the collision complexes are formed with very large angular momentum, as required by the large reaction cross sections, and  $\mathbf{L} + \mathbf{J} \simeq \mathbf{L}$  is essentially perpendicular to  $\mathbf{V}$ , the average period for a forward-to-backward rotation is quite short. This leads to a rough upper limit of  $\sim 5 \times 10^{-13}$  sec for the average lifetime of the collision complex.

Of the reactions studied thus far, only  $\text{M} + \text{CH}_3\text{NO}_2$  appears to give an isotropic product distribution (in the CM system). Further work is required to identify definitely the product; however, magnetic deflection analysis<sup>45</sup> has shown that the product is diamagnetic and it is probably  $\text{MNO}_2$ . If so, it may be significant that this is the only case so far studied in which the product is formed by attack of the M atom on a central atom rather than a peripheral atom.<sup>45</sup> It should also be noted that for several of the reactions which are intermediate between rebound and stripping the product distributions may actually be essentially isotropic. Although the kinematic analysis indicates sideways peaking, for some of these reactions the uncertainty is too large to permit an isotropic distribution to be ruled out. Of course, whereas observation of forward-backward asymmetry points to a direct interaction mechanism, observation of an isotropic distribution cannot be taken as evidence for a statistical complex mechanism since (as illustrated in the discussion of Fig. 17) an isotropic distribution can also result from a direct interaction mechanism.

In the Monte Carlo computer studies the direct interaction mechanism appears to be quite general. Even for potential surfaces which do not give agreement with the beam experiments, it usually is found that most of the trajectories turn the corner smoothly and the products separate within  $5 \times 10^{-13}$  sec or less.<sup>27,33</sup> These results are of particular interest, since in theoretical chemical kinetics much more attention has been given to statistical collision complex models than to direct interaction models.

**Transition between Rebound and Stripping.** The correlation among the magnitude of the reaction cross section, the preferred direction of recoil

of the products, and the form of the wide-angle elastic scattering (properties 2-4) has a simple heuristic interpretation which is illustrated in Figures 17-19. It is convenient to discuss this in terms of a rudimentary extension<sup>47</sup> of the semiclassical optical potential model for elastic scattering.<sup>95</sup> The qualitative features of interest here are definitely not unique to this model, but it nicely simulates some of the results of the Monte Carlo calculations.<sup>32,66</sup> The reactants  $A + BC$  are assumed to approach the region of chemical interaction along a two-body central force trajectory specified by an impact parameter  $b$  and kinetic energy  $E$ . A fraction  $P(b, E)$  of these collisions lead to reaction, and the products  $AB + C$  depart along another two-body trajectory with impact parameter  $b'$  and kinetic energy  $E'$ . The differential scattering cross sections for elastic and reactive scattering then are given by

$$I_E(\theta) = [1 - P(b, E)]d(\pi b^2)/d\omega \quad (6a)$$

$$I_R(\theta') = P(b, E)d(\pi b^2)/d\omega' \quad (6b)$$

where  $\theta(b, E)$  and  $\theta'(b, E)$  are the elastic and reactive scattering angles (directions of recoil of  $A$  and  $AB$ , respectively) and  $d\omega = 2\pi \sin \theta d\theta$  and  $d\omega' = 2\pi \sin \theta' d\theta'$  are the corresponding solid angle elements in the CM system. In reactive collisions the scattering angle is the sum of contributions from the reactant and product portions of the trajectory,

$$\theta' = \theta_r(b, E) + \theta_p(b', E') \quad (7)$$

The lack of a third contribution representing the ABC complex makes apparent the "ultra-direct" character of this model. Further assumptions are required to relate  $b'$  and  $E'$  to  $b$  and  $E$ , as described below. With these relations both the elastic and reactive scattering may be evaluated from the usual semiclassical two-body collision mechanics, once the potentials and the reaction probability function  $P(b, E)$  are specified.

For the rebound reactions, the main contributions evidently come from small impact parameters, since  $(\sigma_r/\pi)^{1/2} \approx 2 \text{ \AA}$ . In this region the elastic scattering is dominated by the "repulsive wall" and in the hard-sphere approximation

$$\theta_r = \arccos(b/R) \quad (8)$$

with  $R$  the sphere radius. Since the switchover to products occurs for configurations with the  $A-B$  and  $B-C$  distances somewhere near the

equilibrium bond lengths, the exit impact parameter  $b'$  must also be small; thus the product interaction will likewise be mainly repulsive, and

$$\theta_p = \arccos(b'/R') \quad (9)$$

If the reaction is supposed to occur for a particular configuration of A—B—C, the relation between  $b$  and  $b'$  is fixed by simple geometry. For linear configurations the relation is one-to-one, as illustrated in Figure 17. For bent configurations, all azimuthal orientations about a

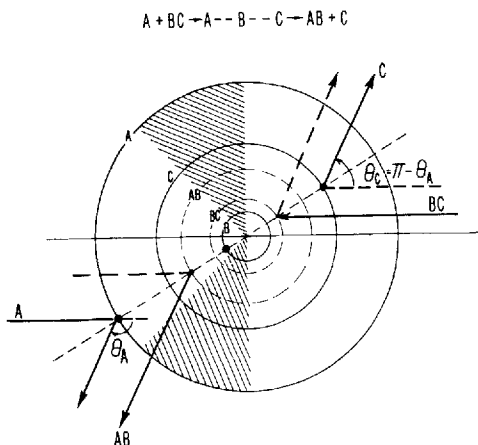


Fig. 17. Relation of elastic and reactive scattering in the primitive optical potential model for a *rebound* reaction. A collinear configuration of ABC is assumed, with both the incoming and outgoing portions of the trajectories governed by hard-sphere repulsion. For an impact parameter such that in elastic scattering the angle of A is  $\theta_A$ , in the reactive scattering the product AB appears at the same angle,  $\theta_{AB} = \theta_A$ , and C at the "mirror image" angle,  $\theta_C = \pi - \theta_A$ . If A is incident on the unshaded area, both A and AB recoil into the backward hemisphere ( $\theta_A \geq 90^\circ$ ) whereas if A is incident on the shaded area they recoil forwards ( $\theta_A \leq 90^\circ$ ).

line from A through the center of mass of BC are equally likely, and this generates a broad spectrum of  $b'$  for each  $b$ ; the averaged scattering evaluated by integrating over the azimuthal orientations closely resembles that for linear configurations, however, as indicated in Figure 18. For  $R \simeq R'$ , this model makes the averaged trajectories for reactively scattered AB approximate specular reflection, roughly parallel to the elastically scattered A. Thus the form factors  $d(\pi b^2)/d\omega$  in Eqs. (6) are

both nearly constant; the angular distribution of reactive scattering is directly determined by  $P(b,E)$ , with  $b = b(\theta')$ , and the wide-angle elastic scattering is determined by  $1 - P(b,E)$ , with  $b = b(\theta)$ . Since for rebound reactions the elastic scattering is found to be very similar to that of nonreactive systems (see Fig. 8), the reaction probability  $P(b,E)$  is evidently well below unity even for small impact parameters. If the reaction can occur only for  $b < R/\sqrt{2}$  (unshaded region in Fig. 17, or average unshaded region in Fig. 18), the distribution of AB is entirely

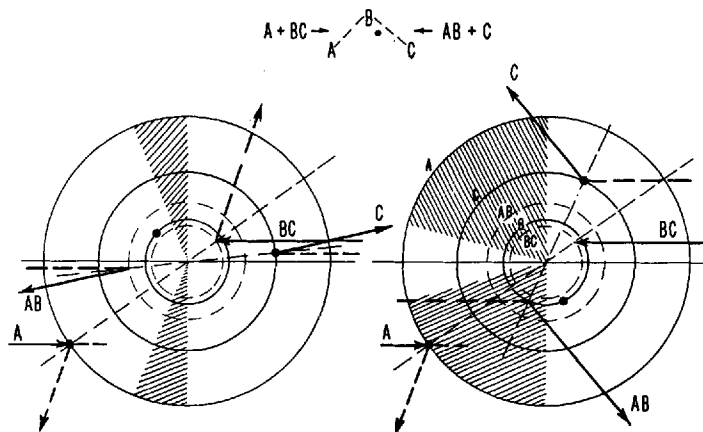


Fig. 18. Primitive rebound reaction model for a bent configuration of ABC. An average must be taken over all azimuthal orientations of the BC axis about the line from A through the center of mass of BC. As illustrated by the two extreme cases pictured here, the relations shown for the collinear case in Fig. 17 are thereby broadened, but the average remains close to the collinear result.

confined to the backward hemisphere, whereas if reaction is equally probable for all impact parameters up to  $b = R$ , the angular distribution of AB becomes nearly isotropic. This same qualitative correlation between the range and form of the reaction probability and the form of the angular distributions has been found in the Monte Carlo calculations for a wide variety of potential surfaces, although the degree to which the wide-angle scattering of A and AB approach specular reflection varies considerably with the potential.<sup>32,66</sup>

For the stripping reactions, the remarkably big cross sections indicate that the reaction probability must be high for collisions with impact parameters as large as  $(\sigma_r/\pi)^{1/2} = 6 \text{ \AA}$  or more. Since there is no evidence

of a repulsive wall contribution in the elastic scattering, the residual wide-angle elastic scattering apparently comes solely from "orbiting" collisions in which the reactants are held apart by a centrifugal barrier (see Fig. 21). In this realm the deflection may be approximated by<sup>96</sup>

$$\theta = 2\theta_r = \theta_0 + a_0 \ln [(b - b_0)/b_0] \quad (10)$$

for  $b > b_0$ , where  $b_0$  is the impact parameter for a trajectory which just reaches the top of the barrier. The corresponding angular distribution, evaluated from Eq. (6b), falls off as  $\exp(-\theta/a_0)$  at wide angles. The decay parameter  $a_0 \simeq 30^\circ$  for any potential which goes as  $r^{-6}$  at long range and is almost independent of the collision energy (as long as  $E$  is within the orbiting realm). The observed wide-angle elastic scattering shows precisely this  $30^\circ$  exponential falloff (dashed line in Fig. 8).

The forward peaking of reactively scattered AB observed in stripping reactions is also readily obtained from the model. Since  $P(b, E)$  is now taken as unity for  $b$  well beyond the hard sphere radius  $R$ , the terms considered for the rebound model, Eqs. (8) and (9), give an isotropic contribution. Superimposed on this are further contributions from the regions with  $b > R$  or with  $b' > R'$  in which attractive forces dominate. Here the deflections  $\theta_r$  or  $\theta_p$  are negative, whereas for  $b < R$  or  $b' < R'$  they were between 0 and  $90^\circ$ . Only the absolute value of the scattering angle,

$$|\theta'| = |\theta_r + \theta_p| \quad (11)$$

is observable and hence the regions in which  $\theta_r$  and  $\theta_p$  differ in sign (i.e.,  $b > R$ ,  $b' < R'$  and  $b < R$ ,  $b' > R'$ ) favor forward scattering. The situation is illustrated in Figure 19, which corresponds to a collision with the reactant part of the trajectory attractive ( $b > R$ ,  $\theta_r < 0$ ) and the product part repulsive ( $b' < R'$ ,  $\theta_p > 0$ ). As is clear from the elastic scattering, contributions with  $b > R$  must be very important, especially since they are heavily weighted by the target area distribution,  $d(\pi b^2)$ . Thus if the reaction cross section is large enough, the AB distribution should be strongly peaked forward. Although it is much weaker, there is also appreciable backward scattering of AB arising from the isotropic contribution. According to the model, the backward scattering should in fact be substantially larger than for rebound reactions, since in the rebound case  $P(b, E)$  is well below unity. This again agrees with the experimental results (see Fig. 9).

The notion that all trajectories which surmount the centrifugal barrier

and reach the "hard collision" region will lead to reaction has been employed in many model calculations of total cross sections for various types of fast reaction processes.<sup>52,97</sup> The observed angular distributions now offer very strong evidence that this is actually the situation for stripping reactions.

For reactions intermediate between rebound and stripping, the prediction of the optical potential model is quite sensitive to the form of the reaction probability function. Thus, the product distribution will be essentially isotropic if  $P(b,E)$  is roughly constant up to a cutoff in the vicinity of  $b \simeq R$ , whereas the distribution can be peaked sideways if  $P(b,E)$  gives less weight to collisions with small impact parameters.

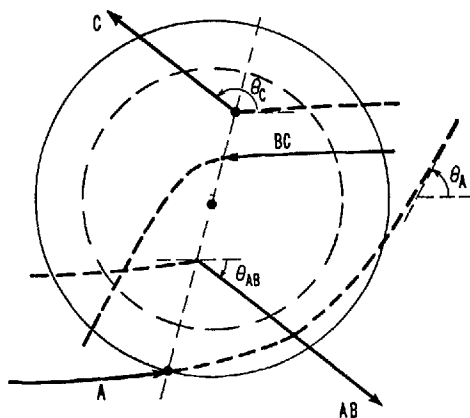


Fig. 19. Primitive optical potential model for a *stripping* reaction, illustrating the forward scattering of AB produced by reaction at impact parameters in the attractive zone (region outside the dashed sphere which represents the repulsive core considered in Figs. 17 and 18).

The proper interpretation of the approximate constancy observed in the sum of elastic and reactive scattering (property 5) is not clear, especially since this property has not yet been examined in the Monte Carlo studies. The optical potential model does not necessarily lead to this result. However, if the scattering functions  $\theta(b,E)$  and  $\theta'(b,E)$  are not very different in form, or if the differences are blurred out by averaging over the velocity distributions, Eqs. (6) imply that the sum of elastic and reactive scattering should be approximately described by a common factor,  $I(\theta) = d(\pi b^2)/d\omega$ , which is independent of the  $P(b,E)$  function.

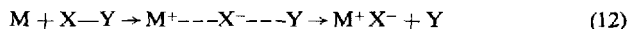
In this case the total scattering in the LAB system would often resemble closely that for similar nonreactive molecules, as is observed, since often the velocity-averaged kinematic transformations (CM  $\rightarrow$  LAB) are approximately the same for the elastic and reactive scattering.

**Other Properties.** Both the facts that the shape of the MX angular distribution (property 6) is much more sensitive<sup>38,42</sup> to the identity of the reactant molecule XY than to the alkali atom M and that the velocity distribution (property 7) is insensitive to changes in the initial collision energy<sup>41,44,47</sup> suggest that these properties are largely determined by the forces which govern the "pulling apart" of the XY molecule. (A specific mechanism for this correlation is discussed in Section II.) As yet, these properties have only been established for a few of the most exothermic stripping reactions (and they may not prove to hold elsewhere). For these reactions the M + XY interaction must be very strong and of long range (as indicated by properties 1-4). Thus a *saturation effect* is to be expected: changes in the range and form of the  $P(b,E)$  function due to changing the identity of M or the initial relative kinetic energy  $E$  will be "washed out" by the powerful acceleration between M and XY and consequently will have little effect on the distribution in angle and velocity of the products.

As discussed already in Section E, the partitioning of angular momentum between orbital and rotational motion in the products (property 8) is also determined by the forces which govern the breakup of the collision complex.

## II. CHEMICAL FORCES IN CHARGE-TRANSFER REACTIONS

The traditional physics professor is supposed to point to chemistry as a monumental demonstration of what can be done with electrons, a few nuclei, and Coulomb's law. He might even be surprised at how much fun can be had in exploring the simplest consequences of "the one-electron problem" in chemical dynamics. According to the electron jump model, the alkali reactions are, in effect, gas-phase acid-base or ion-recombination reactions, as



Michael Polanyi suggested the picturesque term *harpooning* for this process: the attacking alkali atom tosses out its valence electron, hooks the halogen, and hauls it in with the Coulomb force. The basic features

of the mechanism have been developed in a nice theoretical study by Magee.<sup>81,82</sup> Since the contribution of this mechanism depends critically on the energy required to form the ion-pair, it is essential to know or guess the electron affinity of the acceptor molecule.

As the experimental information is very meager and unreliable,<sup>98-100</sup> we have adopted molecular orbital arguments developed by Mulliken and Person for the analysis of charge-transfer spectra.<sup>101</sup> This approach leads to a qualitative correlation between the reaction dynamics and the electronic spectra of the reactant molecule. It also brings out interesting implications of the model which depend intimately on the nature of the orbitals available to the harpooning electron.

### A. The Harpooning Mechanism

The main points in Magee's discussion may be reviewed by reference to Figure 20, which gives the potential curves for the lowest few electronic states of an alkali halide molecule. In the ground state the molecule is essentially  $M^+X^-$  near its equilibrium bond distance and yet

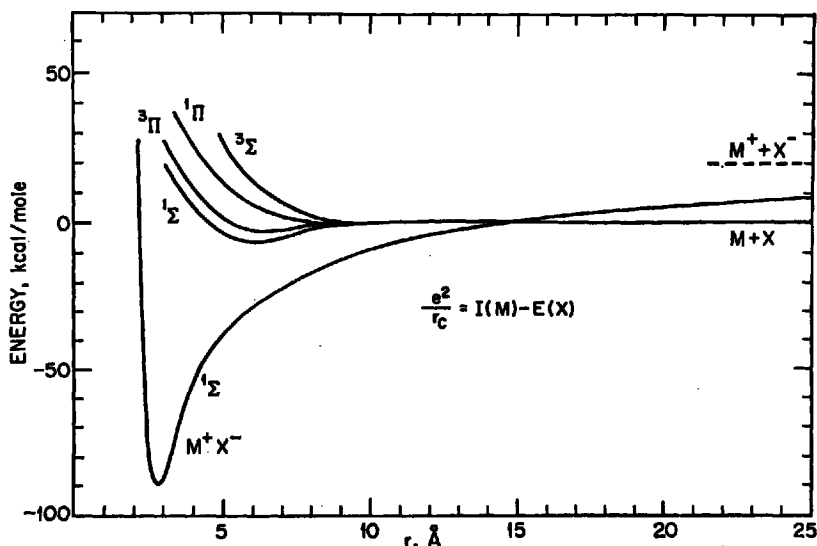


Fig. 20. Potential-energy curves for an alkali halide molecule (drawn for KBr) showing the "zeroth-order crossing" of the ionic and covalent states.

dissociates to form atoms. The zeroth-order potential curve for the "purely ionic" electron configuration therefore must cross that for the "purely covalent" configuration. As these configurations interact to some extent, they are mixed in a higher order of approximation. Hence the potential curves for the stationary states do not cross, but may approach very closely if the configuration mixing is weak.<sup>102</sup> The internuclear distance at the position of the zeroth-order crossing,  $r_c$ , is quite large ( $\sim 15 \text{ \AA}$  for KBr) and since the Coulombic attraction is dominant there,  $r_c$  may be determined from the energy required to form the ion-pair,

$$e^2/r_c \simeq I(M) - E(X) \quad (13)$$

Here  $I(M)$  denotes the ionization potential of the alkali atom and  $E(X)$  the electron affinity of the halogen atom.

For the lowest stationary state, the electron distribution must undergo an abrupt change in the vicinity of  $r_c$ , from dominantly covalent outside to dominantly ionic inside. This corresponds to the jump of the electron from the alkali to the halogen atom. The Born-Oppenheimer approximation has been assumed, and accordingly the stationary states are eigenfunctions of the electronic Hamiltonian with the nuclei clamped in position. However, it should be noted (for later reference) that this approximation may fail if the crossing point occurs at a very large distance and the internuclear distance changes with appreciable velocity. The ionic-covalent configuration mixing will then be very weak and the electron will not have time to jump as the region of the crossing point is traversed. This is actually what occurs for the alkali halides.<sup>103</sup> The optical spectra corresponding to transitions from the ground to the lowest bundle of excited states are continuous rather than discrete as required by the Born-Oppenheimer approximation. The only exceptions are the molecules for which  $r_c$  is smallest (e.g., NaI, with  $r_c \sim 7 \text{ \AA}$ , and possibly LiI and LiBr); the spectra of these show some banded structure.

In an  $M + XY$  reaction the situation is essentially the same.<sup>82</sup> The potential surfaces for the  $M\text{---}X\text{---}Y$  and  $M^+\text{---}X^-\text{---}Y$  electronic configurations must cross, and the electron jump can occur only in the close vicinity of the crossing. The nature of the crossing actually differs from that for the diatomic case, as here even the stationary-state potential surfaces can cross (except for the exactly collinear configuration, for which the "avoided intersection" situation still holds).<sup>104</sup> Also, the

$MX$  distance at the crossing will vary with the position of the  $Y$  group, but again for configurations in which the Coulombic attraction is dominant,

$$e^2/r_c \simeq I(M) - E^v(XY) \quad (14)$$

where  $E^v(XY)$  denotes the vertical electron affinity of the  $XY$  molecule (evaluated at the bond distance which obtains during the electron jump). In most cases,  $r_c$  for  $M + XY$  will be considerably smaller than for  $M + X$ , since very few  $XY$  molecules are expected to have electron affinity comparable to that of an  $X$  atom. Thus the Born-Oppenheimer approximation should usually hold, and most  $M + XY$  reactions are expected to take place on the lowest stationary-state potential energy surface. Of course, both Eqs. (13) and (14) become invalid if the calculated  $r_c$  is so small that Pauli repulsion forces or other interactions become comparable to the Coulomb attraction. In the case of  $M + XY$  reactions for which  $r_c$  does become large enough to inhibit the electron jump, Eq. (14) again must be amended; here the successful electron jumps will tend to become appreciably nonvertical and the vertical electron affinity should be replaced by one averaged over the appropriate portion of the potential curve for the  $XY^-$  ion.

Figure 21 gives an idea of the strength of the "harpoon potential" for interaction of  $M + X_2$  as compared with an ordinary long-range van der Waals potential. We have chosen the convenient functional form

$$V_H(r) = V_I(r) \sin^2 \omega + V_C(r) \cos^2 \omega \quad (15)$$

where the mixing parameter  $\omega$  describes the switchover from the covalent intersection (at  $r > r_c$ ,  $\omega \rightarrow 0^\circ$ ) to the ionic interaction (at  $r < r_c$ ,  $\omega \rightarrow 90^\circ$ ) and

$$\begin{aligned} V_C(r) &= -C/r^6 \\ V_I(r) &= \Delta - e^2/r - \frac{1}{2}e^2(\alpha_1 + \alpha_2)/r^4 - 2e^2\alpha_1\alpha_2/r^7 \\ \omega &= (\pi/4) [1 - \tanh \gamma(r - r_c)] \end{aligned}$$

At the large distances considered here,  $V_C$  is just the usual dispersion force term (with  $C \simeq 5330$  kcal/mole  $\text{\AA}^6$  calculated from the Slater-Kirkwood approximation<sup>105</sup>). For  $V_I$  the Rittner potential<sup>106</sup> for a pair of polarizable ions is used. The parameter  $\Delta = e^2/r_c$  is the energy required to form the ion-pair, as in Eq. (14), and the parameter  $\gamma$

prescribes the abruptness of the switchover; for this example we have arbitrarily taken  $\Delta = 50$  kcal/mole and  $\gamma = 1 \text{ \AA}^{-1}$ . The comparison potential (dashed curve) is an Exp-6 ( $\alpha = 12$ ) function; the parameters are taken from scattering data for the  $\text{K} + \text{HBr}$  system.<sup>12</sup>

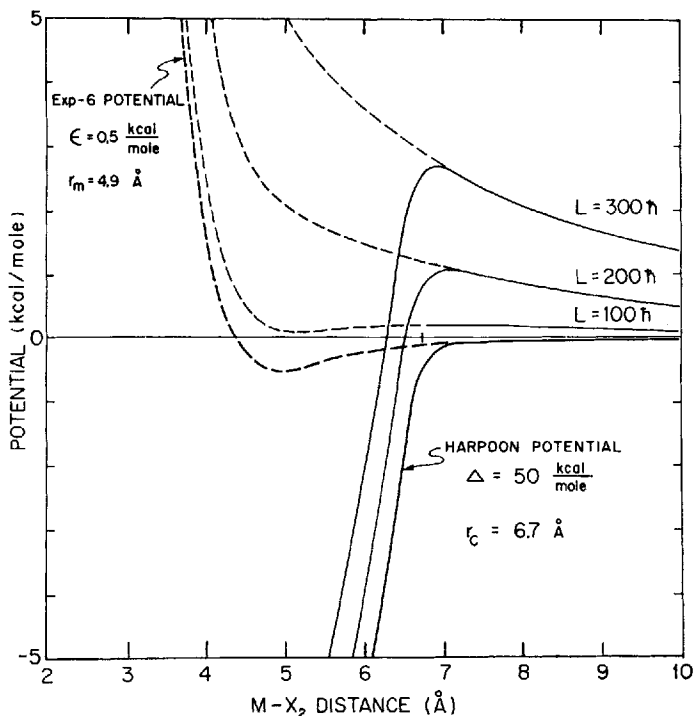


Fig. 21. Comparison of the effective potential energy curves (including the centrifugal repulsion term) for collision of  $\text{K} + \text{Br}_2$  subject to ordinary van der Waals forces (dashed curves) or to the harpoon potential (solid curves).

Figure 21 also shows several of the effective potential curves which include the centrifugal repulsion term,  $L^2/2\mu r^2$ . These curves indicate the special role played by the centrifugal barrier for a screened Coulomb potential. For ordinary intermolecular potentials, qualitatively similar to the Exp-6 function, the position of the centrifugal barrier varies rapidly with the orbital angular momentum. Above a particular value ( $L \approx 125 \hbar$  for this example) the centrifugal repulsion energy overcomes the attractive interaction and the effective potential curve becomes

monotonic. In contrast, when the attraction is Coulombic, the more slowly varying centrifugal term can never introduce a maximum. Thus for a screened Coulomb potential the centrifugal barrier is always confined to the switchover region. The location of the barrier is only weakly dependent on the angular momentum and its shape is largely determined by the width and form of the switchover function. Also, the effective potential curves for the harpoon potential cannot become monotonic until the centrifugal energy at  $r_c$  becomes of the order  $\frac{1}{2}\Delta$  (or  $L \sim 800 \hbar$  for our example).

In reactions for which  $r_c$  is large enough to make Eq. (14) a fair approximation, just before the electron jump the  $X_2$  molecule is nearly unaware of the presence of the M atom. Thus the arrival of the harpooning electron produces a Franck-Condon transition between the potential curves for the isolated  $X_2$  and  $X_2^-$  molecules, as indicated in Figure 22. The  $X_2^-$  curve of course only defines the initial stage in the formation of the final products; as  $M^+$  approaches,  $X_2^-$  is severely distorted by the strong electric field and dissociates. In the case pictured in Figure 22 the  $X_2^-$  ion is formed in a highly excited vibrational state, barely

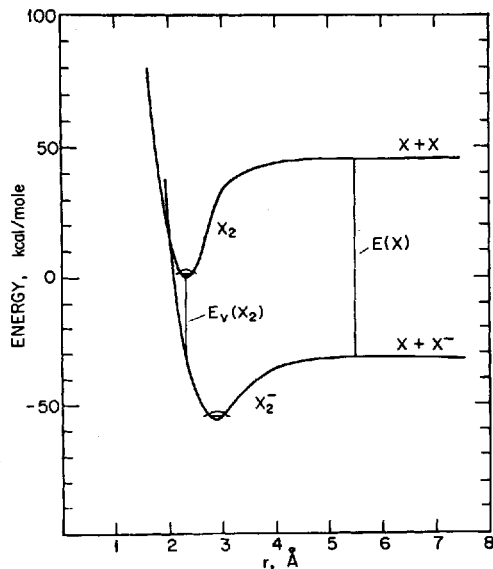


Fig. 22. Potential-energy curves for the ground electronic states of a diatomic halogen molecule and its negative ion (drawn for  $Br_2$ ).

below the dissociation limit. Such an ion will readily break up in the electric field, which will exceed  $3 \times 10^9$  V/cm when  $M^+$  approaches within 7 Å. External fields of the order of  $10^6$  V/cm have been shown to produce efficient dissociation of free, vibrationally excited  $H_2^+$  ions.<sup>107,108</sup>

The lag between the arrival of the harpooning electron and that of  $M^+$  can be appreciable. For example,  $K^+$  and  $Br_2^-$  ions starting 7 Å apart at rest and with no orbital angular momentum require  $\sim 10^{-13}$  sec to reach 3 Å, the vicinity of the  $K^+Br^-$  equilibrium bond distance. The lag is only slightly shortened by the addition of initial thermal velocity, and with orbital angular momentum it becomes longer; for example,  $\sim 2 \times 10^{-13}$  sec for  $L \sim 200 \hbar$ . For the case of Figure 22, the time required for the breakup of  $X_2^-$  is less than the vibrational period, or  $\approx 10^{-13}$  sec. Thus, when the  $M^+$  ion is delayed by centrifugal repulsion, it may find that only the  $X^-$  ion is at the scene as the X atom has already departed.

It should be emphasized that the harpooning mechanism has many variations. Although the main features are determined essentially just by the vertical electron affinity, many details of the reaction dynamics will differ with the shape and particularly the location of the asymptote of the potential curve for the negative molecule ion. (Some of the possibilities are classified in Figure 28.) In many reactions the negative ion will be formed in a purely repulsive state, or above the dissociation asymptote of an attractive state; in others it may appear in a low vibrational level of a state that would be stable if the electric field were not present. Thus the case of Figure 22 is quite special, although hopefully it is qualitatively correct for the diatomic halogen systems. The rough approximations<sup>101</sup> used to estimate the curve for  $X_2^-$  will be discussed later.

Also, it should be noted again that for large  $r_c$  the electronic transition is not vertical. This occurs with respect to the  $M-X_2$  distance because the nuclei have some time to move while the electron makes its long-distance hop. It occurs also with respect to the  $X-X$  distance because the jump will incline to favor smaller electron affinity and thereby decrease  $r_c$  (see Fig. 24).

The harpooning model obviously offers ready qualitative explanations<sup>39,42,47,89</sup> for the main features of the reaction dynamics: the high level of product internal excitation arises because the potential surface is extremely attractive within the crossing radius; the impulsive interaction

mechanism is a Franck-Condon transition from a reactant to a product trajectory; the correlations associated with the transition between the rebound and stripping limits simply reflect the range over which the Coulombic attraction operates, as determined from Eq. (14). Here we shall only comment briefly on a few aspects of experimental tests of the harpooning mechanism.

**Total Reaction Cross Section.** There seems to be no other mechanism which can account for the very large cross sections found in the flame studies<sup>78</sup> of the  $\text{Na} + \text{X}_2$  system ( $\sigma_r \sim 50\text{--}75 \text{ \AA}^2$ ) and the beam studies<sup>28,42</sup> of the  $\text{K}, \text{Rb}, \text{Cs} + \text{X}_2$  systems ( $\sigma_r \sim 200\text{--}250 \text{ \AA}^2$ ). As seen in Figure 21, the centrifugal barrier remains very close to the crossing point, so that for harpooning  $\sigma_r$  is approximately given by  $\pi r_c^2$  and should be nearly independent of energy. Figure 23 shows the dependence

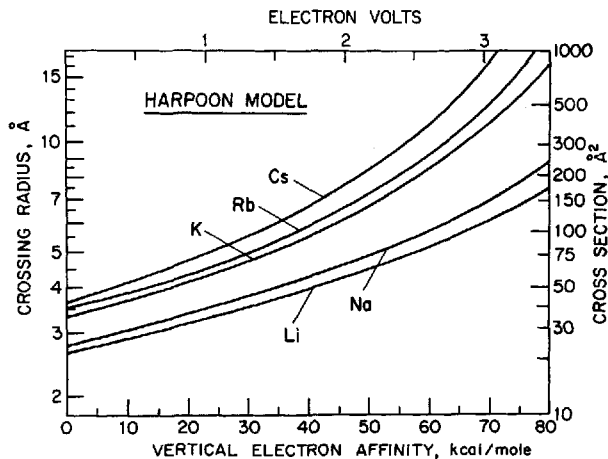


Fig. 23. Variation of the crossing radius,  $r_c$ , and the reaction cross section,  $\sigma_r \simeq \pi r_c^2$ , with the vertical electron affinity of the electron acceptor according to the harpoon model.

on the vertical electron affinity, according to Eq. (14). The model appears to be compatible with both the flame and the beam results, although the value indicated for the vertical electron affinity ( $\sim 50$  kcal/mole) is considerably higher than the estimates<sup>101</sup> to be discussed later. The systematic error in  $\sigma_r$  for both sets of experiments could easily be larger than the traditional factor of 2; it would be very desirable to have beam results on  $\text{Na} + \text{X}_2$  for comparison. Also, the increase

in  $\sigma_r$ , predicted on going from K to Cs (for fixed  $X_2$ ) is not apparent in the present beam data. Possibly, this might arise from the saturation effect which is expected to appear in  $\sigma_r$ , when  $r_c$  becomes large enough to inhibit the electron jump; the spectra of the alkali halides<sup>103</sup> suggests that this is likely to occur in the vicinity of  $r_c \sim 7 \text{ \AA}$ .

**Energy Disposal.** The Monte Carlo calculations show that high internal excitation in the products is evidence only for an early downhill potential and harpooning need not be invoked. Nonetheless, harpooning is very likely the chemical basis. An excellent detailed discussion has been given recently by J. C. Polanyi.<sup>89</sup> He was particularly concerned to show that the repulsion which appears between  $X^-$  and Y in Eq. (12) just after the electron jump need not show up in translational acceleration of the Y group with respect to  $M^+X^-$ . He pointed out that because of the Coulombic attraction between  $M^+$  and  $X^-$  the momentum imparted to  $X^-$  in repulsion from Y will induce a momentum of opposite sign in  $M^+$  and thus enhance the vibrational excitation rather than translational recoil. Computer studies have borne this out.<sup>109</sup> It may be noted that his discussion does not refer to the situation indicated in Figure 22 but to the case of a monotonic repulsive  $XY^-$  potential curve which is everywhere above the dissociation asymptote (labeled as case I+C in Fig. 28). As we have seen for the Figure 22 case, the initial repulsion between  $X^-$  and Y will be relaxed very quickly and often their interaction will be attractive (or perhaps nil) by the time  $M^+$  arrives.

Figure 24 gives an example of a potential energy surface derived from the harpoon model. The construction of this surface is described elsewhere<sup>49</sup>; it is similar to the procedure used in the first Monte Carlo calculations<sup>14,32</sup> except that terms involving the ions were brought in as in Eq. (15). The essential aspect of an early downhill surface which traps a large fraction of the exothermicity as vibrational excitation is that the attraction in the bond being formed is maintained until any appreciable repulsion between the products is dissipated.<sup>89,109</sup> As expected, the surface of Figure 24 nicely exemplifies this.

The surface also illustrates a rather peculiar feature of harpooning which may permit a specific experimental test of the mechanism. As shown by the dashed curve, the nominal jumping radius  $r_c$  varies quite rapidly with the Br—Br distance. As before,  $r_c$  was evaluated from Eq. (14), now using at each Br—Br distance (denoted by  $r'$ ) the value of the vertical electron affinity obtained from the difference of the  $\text{Br}_2$  and  $\text{Br}_2^-$  potential curves in Figure 22. The affinity varies from near

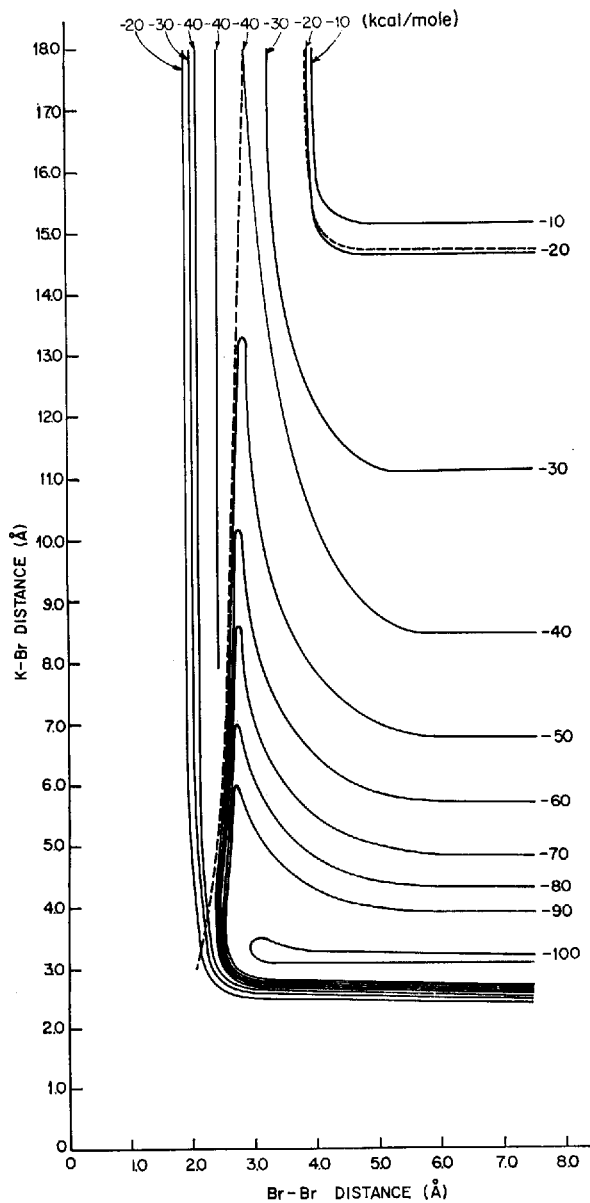


Fig. 24. Potential-energy surface for linear configurations of the K-Br-Br system, as derived from the harpoon model and the molecular potential curves of Figures 20 and 22. The solid curves are contours of constant energy; the energy zero corresponds to infinite separation of the three atoms. The dashed curve shows the variation of the crossing radius  $r_c$  with the Br-Br distance.

zero at  $r' = 2 \text{ \AA}$  to 25 kcal/mole at the equilibrium bond distance  $r' = 2.28 \text{ \AA}$  for  $\text{Br}_2$  and reaches a maximum of 89 kcal/mole at  $r' = 3.1 \text{ \AA}$ . Thus if energy were supplied to prestretch the Br—Br bond, electron jumps would become possible at considerably larger values of  $r_c$  than that corresponding to the equilibrium  $\text{Br}_2$  bond distance. Again, if  $r_c$  becomes too large, breakdown of the Born-Oppenheimer approximation would inhibit the jumps and make them nonvertical. If the cross sections for  $\text{M} + \text{X}_2$  and other stripping reactions are indeed near the upper limit allowed by the Born-Oppenheimer breakdown, these may not be sensitive to initial vibrational excitation of the reactant molecule. However, if harpooning is also important for rebound and intermediate reactions these would be expected to be sensitive to initial vibrational excitation.

**Angular Distributions.** The evidence for orbiting<sup>38,42,43</sup> in the wide-angle elastic scattering of  $\text{M}$  from  $\text{X}_2$  and other stripping reactions and the lack of rainbow structure<sup>4,28,43</sup> indicate that attenuation by reaction must be very strong up to distances of at least 6–7  $\text{\AA}$ . Even the very small angle elastic scattering<sup>30</sup> shows appreciable deviations from the pattern for comparable nonreactive molecules which indicate some deviation from the usual  $r^{-6}$  van der Waals force at distances up to  $\sim 15 \text{ \AA}$ . Again, it seems necessary to invoke ionic interactions to account for these observations. A particularly inviting prospect for further elastic scattering studies is apparent from Figure 21. Measurement of the velocity dependence of the scattering at collision energies well above those for which ordinary van der Waals orbiting is possible should show whether the centrifugal barrier persists in the vicinity of  $r_c$  and might give some information about the form of the switchover function. Some data of this kind is already available,<sup>28,43</sup> but it has not yet been analyzed in terms of the harpoon potential.

The observation<sup>38,42</sup> that for several stripping reactions the shape of the angular distribution of reactively scattered  $\text{MX}$  is much more sensitive to the identity of  $\text{XY}$  than to  $\text{M}$  fits in nicely with the harpooning picture. This would be expected to occur whenever  $r_c$  is large and the  $\text{XY}^-$  ion breaks up readily. The initial state of the  $\text{XY}^-$  ion and its resistance to decomposition may be quite different even for similar molecules, since they depend on the potential curves, whereas if  $r_c$  is large the shift in  $r_c$  due to changing the identity of  $\text{M}$  has little effect except to alter somewhat the electric field acting on  $\text{XY}^-$  as it breaks up.

**Basis for Spectator Model.** In nuclear stripping reactions<sup>110,111</sup> of the

type  $A + BC \rightarrow AB + C$ , the characteristic feature is that the incident particle  $A$  interacts impulsively with only part  $B$  of the target. The products separate before there is time to transfer any momentum to the rest of the target, so that  $C$  just plays the role of a spectator. In this situation, once the interaction sets in,  $A + B$  and  $C$  behave as separate dynamical systems. Thus the final momentum carried by the product  $AB$  is given by the momentum of the center of mass of  $A + B$  just before the collision, or

$$m_{AB}C_{AB} = m_A v_A + m_B C_{BC} + \mu_{BC}(v_B - v_C) \quad (16)$$

The second term is the momentum  $B$  acquires from motion of the center of mass of  $BC$ . The third is the internal momentum of  $B$  in vibrational and rotational motion relative to the center of mass of  $BC$  and  $\mu_{BC} = m_B m_C / m_{BC}$  is the reduced mass of  $BC$ . The recoil momentum of  $AB$  relative to the center of mass of the whole system is thus given by

$$m_{AB}(C_{AB} - C) = (m_A m_C / M) V + \mu_{BC}(v_B - v_C) \quad (17)$$

where  $M$  is the total mass and  $V = v_A - C_{BC}$  is the initial relative velocity of approach of  $A$  to  $BC$ . From Eq. (17) we see that this model always makes the distribution of  $AB$  recoil vectors peak forward along  $V$ , as the internal momentum distribution is isotropic. If the initial conditions are well enough defined to make the spread in  $V$  negligible, the observed breadth and shape of the angle and velocity distributions of  $AB$  are simply determined by the internal momentum distribution within  $BC$  just before reaction.

There is evidence that at high kinetic energies ( $> 5$  eV) some proton transfer ion-molecule reactions conform to the spectator model.<sup>112</sup> At these energies this is plausible since the time scale for the external interaction of  $A + BC$  is much shorter than that for communication of momentum within  $BC$ . At lower energies the same reactions appear to proceed mainly by a collision complex mechanism.

The spectator model is also at least qualitatively useful for alkali atom stripping reactions. In the Oak Ridge study of the  $Cs + Br_2$  reaction,<sup>28</sup> it was found that the location of the peak of the  $CsBr$  angular distribution and the slight forward shift and narrowing observed with increase of the  $Cs$  velocity agreed nicely with the spectator model. In this comparison the internal momentum term of (16) and (17) was not included. However, it has since been found that with this term the spectator model gives fairly good agreement for most of the alkali atom stripping reac-

tions thus far studied.<sup>40,41</sup> In particular, a detailed comparison has been made with the results obtained in the velocity analysis experiments on the  $K + Br_2$  reaction.<sup>41,44</sup> A plausible assumed form for the internal momentum distribution can account for the observed approximately Maxwellian shape of the  $KBr$  velocity distributions, the variation with angle, and the insensitivity to the  $K$  velocity. Thus the present evidence for spectator dynamics in alkali reactions is substantial, although not conclusive because of the kinematic limitations in analysis of the data.

The spectator model would seem to be out of the question for ordinary thermal reactions, as the times required for external and internal momentum transfers are too nearly comparable. The appearance of apparent spectator dynamics here may be understood as another aspect of the harpooning mechanism. Merely switching on the Coulomb interaction of  $M^+$  and  $X^-$  does not establish spectator conditions; even if  $M^+$  is too far away to interact appreciably with  $Y$ , the interaction of  $X^-$  with  $Y$  ordinarily cannot be neglected. Thus in general a momentum transfer term must be added to Eqs. (16) and (17). However, if  $r_c$  is large the breakup of the  $XY^-$  ion often will be practically complete while  $M^+$  is still far away. This isolates  $Y$  and thereby fixes the momentum transfer. Essentially, Eqs. (16) and (17) can be used again but with the external terms fixed before the electron jump and the internal term fixed after the breakup of  $XY^-$ . In the case considered in Figure 22, the net momentum transfer is expected to be relatively small, since the initial repulsion between  $X^-$  and  $Y$  is largely compensated by subsequent attraction. In this case  $E^v(XY) \simeq E(X) - D(XY)$  and the energy required to form  $M^+ + XY^-$  is essentially the same as to form  $M^+ + X^- + Y$ . In the more likely cases where this does not hold, the momentum transfer is apt to be larger.

### B. Correlation with Electronic Structure

The analogy between the electron jump mechanism for alkali reactions and the theory of charge-transfer spectra is very close. The jumping condition of Eq. (14) corresponds to the workhorse approximation<sup>113-115</sup> for the frequency of the charge-transfer band,

$$h\nu_{CT} = I_D^v - E_A^v + \Delta G + \Delta X \quad (18)$$

where  $I_D^v$  is the vertical ionization potential of the free donor molecule,  $E_A^v$  is the vertical electron affinity of the acceptor and  $\Delta G$  and  $\Delta X$  account for other interactions which influence the formation of the

charge-transfer complex. The transition between the ionic and covalent states of MX shown in Figure 20 is a primitive example of a charge-transfer transition.<sup>115,116</sup> Thus, many aspects of the extensive valence theory of charge-transfer complexes are of interest in exploring the chemical implications of the harpooning mechanism. Here we shall only consider what can be inferred about the  $X_2^-$  ions and a few others by applying simple molecular orbital arguments, coupled with spectroscopic and electron impact data where possible.

**Diatomic Halogens.** Complexes with  $I_2$  are among the most thoroughly studied charge-transfer systems.<sup>101,114</sup> Several methods of analysis based on Eq. (18) have been used to deduce values of  $E^v(I_2)$  from the spectra of various complexes. The results are in the range  $E^v(I_2) \sim 15\text{--}45$  kcal/mole. These charge-transfer analyses have been discussed fully by Person.<sup>101</sup> He has also offered semiempirical estimates of some of the  $I_2^-$  potential curves and we shall briefly review this part of his paper.

In molecular orbital theory the electronic configuration of the ground state of  $I_2^-$  is given by

$$\dots \sigma_g^2 \pi_u^4 \pi_g^4 \sigma_u \quad (19)$$

Only the orbitals made from the valence shell  $p$  orbitals of the atoms are shown. The  $\sigma_g$  (bonding) and  $\sigma_u$  (antibonding) orbitals are formed by constructive and destructive overlap of the atomic  $p_z$  orbitals; the  $\pi_u$  and  $\pi_g$  orbitals from overlap of the atomic  $p_x$  and  $p_y$  orbitals. The configuration (19) differs from  $I_2$  only in the additional electron in the strongly antibonding  $\sigma_u$  orbital. In  $I_2$  the  $\pi_u$  orbital is considered to be somewhat bonding, the  $\pi_g$  orbital somewhat antibonding.<sup>117</sup> Since both are filled, their net effect is probably nearly nonbonding, so that in  $I_2^-$  the bonding effect of the two  $\sigma_g$  electrons is partially cancelled by the one  $\sigma_u$  electron. Therefore we can expect that the ground state of  $I_2^-$  will be stable<sup>82,117</sup> and, as a first approximation, the dissociation energy will be about one-half that for  $I_2$ , or  $D(I_2^-) \sim 18$  kcal/mole.

Various semiempirical rules and analogies<sup>101,117</sup> can be used to estimate the equilibrium bond length and vibrational frequency for  $I_2^-$ . For example,  $r_e(I_2^-)$  must be between 4.3 Å (the sum of the van der Waals radii for two I atoms) and 2.67 Å ( $r_e$  for  $I_2$ ). A literal interpretation of the "half-bond" expected for  $I_2^-$  would suggest a value halfway between these, or  $r_e(I_2^-) \sim 3.5$  Å; other estimates indicate a somewhat smaller value.<sup>117</sup> For the symmetrical  $I_3^-$  ion the experimental result is 2.90 Å and this should be a lower limit for the bond length in  $I_2^-$ .

The most useful and convincing way<sup>101</sup> to estimate the properties of  $I_2^-$  is to appeal to the known properties of a suitable excited electronic state of  $I_2$ . The  $^3\Pi_{0u}$  excited state of  $I_2$  has the configuration

$$\dots \sigma_g^2 \pi_u^4 \pi_g^3 \sigma_u \quad (20)$$

which differs from that for the ground state of  $I_2^-$  only in that one of the weakly antibonding  $\pi_g$  electrons is missing. If the antibonding character of this orbital is weak enough, the properties of  $I_2^-$  would be expected to be very similar to those found for  $I_2$  in the  $^3\Pi_{0u}$  state, namely: bond length,  $r_e = 3.02 \text{ \AA}$ ; vibrational frequency,  $\omega_e = 128 \text{ cm}^{-1}$ ; bond strength,  $D = 12 \text{ kcal/mole}$ .

From such considerations Person derived a rough estimate of the potential curve for the ground  $^2\Sigma_u^+$  state of  $I_2^-$ . This is shown in Figure 25 along with curves for several excited states. The position of the asymptote for dissociation to  $I + I^-$  relative to the asymptote for  $I + I$  is accurately known from the electron affinity of the I atom,  $E(I) = 70.6 \text{ kcal/mole}$ .<sup>118</sup> Person constructed the rest of the  $^2\Sigma_u^+$  potential curve

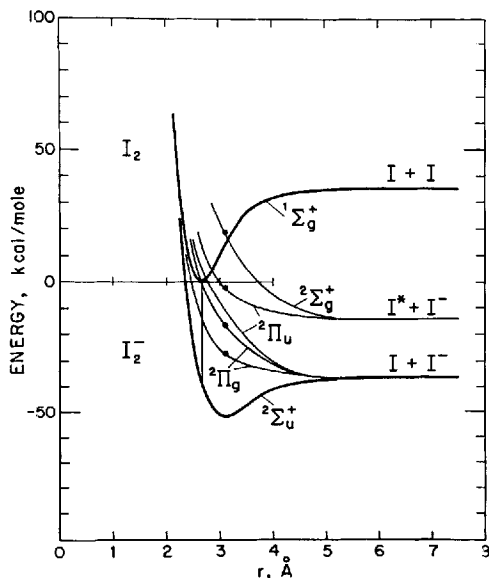


Fig. 25. Potential-energy curves for the ground electronic state of  $I_2$  and several of the lowest group of electronic states of  $I_2^-$ .

by fitting a Morse function to this asymptote and his estimates of the parameters characterizing the minimum. The curve for  $\text{Br}_2^-$  shown in Figure 22 was estimated in the same way. Comparison of the  $\text{X}_2^-$  curve with that for  $\text{X}_2$  gives the electron affinity as a function of the X—X distance. The value obtained for the vertical affinity is 37 kcal/mole for  $\text{I}_2$  and 25 kcal/mole for  $\text{Br}_2$ . These estimates must be assigned an uncertainty of at least  $\pm 10$  kcal/mole because of the uncertainty in the  $\text{X}_2^-$  parameters and the use of the Morse function.

The curves for the excited states of  $\text{I}_2^-$  are repulsive since these states all involve electronic configurations with two electrons in the antibonding  $\sigma_u$  orbital. Figure 26 indicates the correlation of these states with

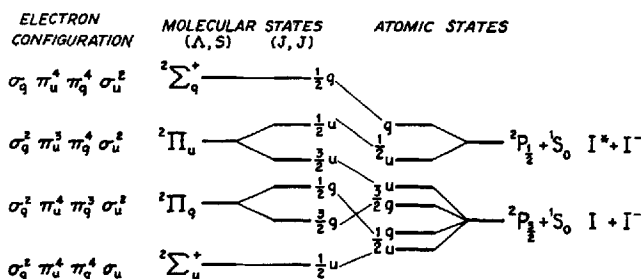


Fig. 26. Correlation of electronic states of the  $\text{I}_2^-$  ion and its dissociation products.

the two possible dissociation asymptotes ( $\text{I} + \text{I}^-$  and  $\text{I}^* + \text{I}^-$ , the latter corresponding to excitation of the atom to the metastable  ${}^2P_{1/2}$  state). The correlations are readily established by matching the  $u, g$  character and the value of the component of the total electronic angular momentum along the internuclear axis for the various possible atomic and molecular states.<sup>119</sup> The location of the excited-state potential curves above the minimum for the ground state has been derived from a study of certain color centers in doped alkali halide crystals.<sup>120</sup> The paramagnetic resonance spectra and the relative intensity and polarization behavior of the various absorptions observed in the optical spectra of these centers show exactly the properties expected for  $\text{X}_2^-$  ions. Thus this study gives the vertical energy differences between the curves for several of the excited electronic states and the potential minimum for the ground state. Flash photolysis of aqueous and ethanolic solutions of alkali halides

also gives rise to spectra that have been assigned to the  $X_2^-$  ions.<sup>121</sup> The results are summarized in Figure 27 and the positions of the states above the minimum are indicated by the dots placed on the curves of Figure 25.

The results of electron impact experiments on the halogens<sup>122,123</sup> have sometimes been regarded as indicating very small (or even somewhat negative) values for the vertical electron affinity. However, these experiments actually only show that the potential curve for some state of  $X_2^-$  must cross that of the ground state of the parent molecule near

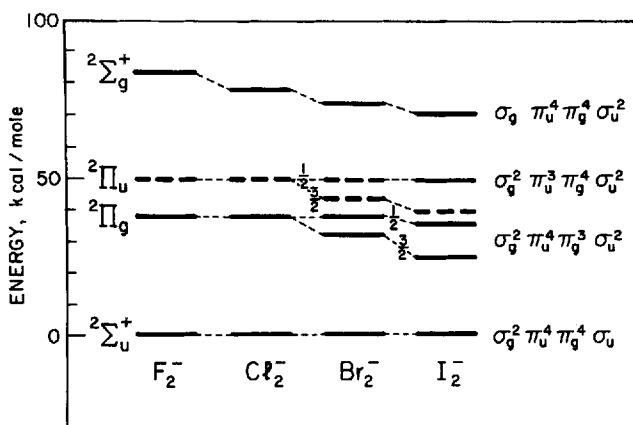


Fig. 27. Location of excited electronic states of the diatomic halogen molecule ions, as derived from spectra of color centers in alkali halide crystals. Transitions involving the levels shown by dashed lines have not been observed.

the minimum in the  $X_2$  curve. There are several candidates for such a state among the excited electronic states of  $X_2^-$ , as seen in Figure 25 (although the uncertainty in the location of the curves is much too large to permit a definite assignment to be made). In the experiments,  $X_2^-$  ions are not found; the only low-energy process observed is dissociative electron capture to form  $X + X^-$  (or possibly  $X^* + X^-$ ). This is just what would be expected from Figure 25, since a stable  $X_2^-$  ion cannot be formed without some way of disposing of the considerable energy released in the electron capture (equal to the vertical electron affinity). The formation of stable negative molecule ions by direct electron capture is rare and appears to occur only for polyatomic

molecules large enough that the exothermicity can be taken up in vibrational excitation.<sup>99,124</sup> Observation of stable  $X_2^-$  ions formed in fragmentation of larger molecules has been reported.<sup>125</sup>

Despite the lack of a direct determination and the wide latitude in quantitative estimates, all the present evidence is compatible with the large values of  $E^v(X_2)$  required by the harpooning mechanism for the  $M + X_2$  reactions. It is also interesting to note what Figure 25 suggests concerning the possible role of the excited electronic states of  $X_2^-$  in these reactions. These states may not contribute at all. For all of them the jumping radius is well within that for the ground state, since  $E^v(X_2)$  is much smaller. Thus if the reaction always occurs at the outermost radius  $r_c$ , the intermediate  $X_2^-$  ion will never be formed in an excited electronic state. In Figure 25 it is apparent that the states which could yield an excited  $I^*$  atom are particularly unfavored and this may be why no sign of  $I^*$  is found in these reactions. The best opportunity for participation of excited electronic states will occur when  $r_c$  for the ground state is so large as to inhibit the electron jump.<sup>82</sup> Accordingly, electronic excitation is more likely to be found for reactions of Cs atoms than for Na atoms (see Fig. 23).

It is conceivable that the probability of reaction by harpooning may depend on the orientation of the molecule in a way characteristic of the symmetry of the electronic state of the negative molecule ion. Recently, Dunn has given general arguments, based on group theory, which show that in many cases the probability of electron capture processes should exhibit a strong dependence on the relative orientation of the axis of the molecule and the incident electron beam.<sup>126,127</sup> His selection rules, if blithely carried over to harpooning reactions, predict that for parallel alignment of the parent  $X_2$  molecule in its  $\Sigma_g^+$  ground state the  $X_2^-$  ion can only be produced in the  $\Sigma_u^+$  or  $\Sigma_g^+$  states, and for perpendicular alignment only in the  $\Pi_u$  or  $\Sigma_g^+$  states. For oblique alignments, all the states can be formed.

**Other Molecules.** The electronic structure of the negative  $XY^-$  ion formed in harpooning can be discussed in much the same way for many of the other reactant molecules in Table I. For most of these a detailed analysis of the molecular orbitals and the electronic spectrum of the parent molecule may be found in a very useful paper by Walsh.<sup>128</sup> As examples we will consider here only a few of the simplest cases, including methyl iodide, the hydrogen halides, and nitrogen dioxide. A convenient qualitative classification of the types of  $XY^-$  potential curves which may

occur is given in Figure 28. The category I or II is decided by the relative magnitude of the bond strength  $D(XY)$  of the parent molecule and the affinity  $E(X)$  of the atom which eventually acquires the electron. In both cases A and B, the free  $XY^-$  ion is stable, but for B as well as the unstable case C the vertical transition leads to immediate dissociation. As we have seen, the ground states of the  $X_2^-$  ions may belong to either case  $I^+A$  or  $I^+B$ .

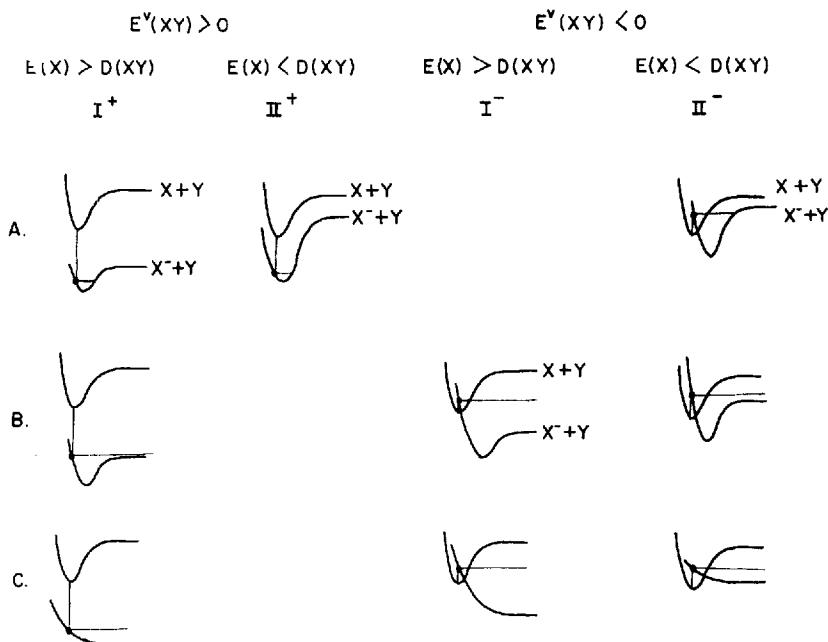


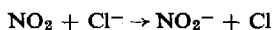
Fig. 28. Classification of electron impact processes producing negative molecule ions ( $XY + e \rightarrow XY^-$ ).

For methyl iodide the complete molecular orbital description<sup>128</sup> is complicated but the features relevant here are closely analogous<sup>129</sup> to the diatomic halogen case. In the united atom approximation the  $CH_3$  group shrinks into an F atom. Thus in diatomic notation the upper occupied orbitals in  $CH_3I^-$  may be denoted by  $\dots \pi^4 \bar{\sigma}$ , as in Eq. (19). Here the  $\pi$  orbital essentially consists of the  $5p_x$  and  $5p_y$  orbitals of the I atom and is approximately nonbonding,<sup>129</sup> whereas the  $\bar{\sigma}$  orbital is

strongly antibonding. In the spectrum of  $\text{CH}_3\text{I}$  the transition to the excited electronic state corresponding to the configuration  $\dots \pi^3 \bar{\sigma}^2$ , analogous to Eq. (20), is well known.<sup>128-130</sup> In contrast to the  $\text{X}_2$  case, this state is repulsive and leads to photodissociation of the molecule. The location and shape of this repulsive curve as derived from the absorption spectrum and the parameters  $D(\text{CH}_3-\text{I}) = 55$  kcal/mole,  $E(\text{I}) = 70.6$  kcal/mole require that the ground state of  $\text{CH}_3\text{I}^-$  be assigned to case I-C of Figure 28. The value indicated<sup>48</sup> for the vertical electron affinity is  $E^v(\text{CH}_3\text{I}) \simeq -20 \pm 20$  kcal/mole. Although this estimate is very rough, the qualitative result seems quite certain. It offers a very plausible explanation of why the  $\text{M} + \text{CH}_3\text{I}$  reactions proceed by a rebound mechanism rather than by stripping.

For the hydrogen halides the topmost occupied orbitals and electronic spectra are somewhat similar to those for  $\text{CH}_3\text{I}$ . The rough arguments again give plausible results but here they are not needed, as the potential curves for the  $\text{HX}^-$  ions can be derived from a recent electron impact study.<sup>131</sup> In this case the observed electron capture must give the ground state of  $\text{HX}^-$  rather than an excited electronic state, as only the ground state correlates with  $\text{H} + \text{X}^-$ . All of these molecules belong to case II-C of Figure 28. The  $\text{HX}^-$  curves are evidently rather flat near the minimum in the  $\text{HX}$  potential and  $E^v(\text{HX}) \simeq E(\text{X}) - D(\text{HX})$  with  $E^v(\text{HX}) \sim -18, -8, \text{ and } 0$  kcal/mole for  $\text{HCl}, \text{HBr}, \text{ and } \text{HI}$ . Thus it is clear that in the  $\text{M} + \text{HX}$  reactions a harpooning reaction could not occur except at distances well within the van der Waals radius, in agreement with the evidence from the elastic scattering studies.<sup>43</sup>

Nitrogen dioxide offers an intriguing example for study of the harpooning mechanism.<sup>45</sup> There is abundant spectral evidence to confirm the close analogy between the electronic structure of the  $\text{NO}_2^-$  ion and the  $\text{O}_3$  molecule,<sup>128,132</sup> and the  $\text{NO}_2^-$  ion is well known in mass spectroscopy. Thus this ion is very stable and belongs to case II+A of Figure 28. Although the electron affinity of the  $\text{NO}_2$  molecule must be very high, no reliable measurements are yet available.<sup>98-100</sup> However, a rigorous lower limit is set by the observation that the charge exchange reaction



occurs at very low energies.<sup>133</sup> This requires that  $E^v(\text{NO}_2) > E(\text{Cl}) = 83$  kcal/mole, and therefore in electron capture  $\text{NO}_2$  acts as if it were a

“super-halogen atom.” Consequently in the  $M + \text{NO}_2$  reactions, the crossing radius will come at an extremely large distance ( $r_c > 20 \text{ \AA}$  for  $\text{K} + \text{NO}_2$ ), larger even than that for an alkali halide molecule (see Fig. 20). The electron jump thus cannot take place to form the ground state of  $\text{NO}_2^-$ , except perhaps in the Na or Li reactions ( $r_c > 8 \text{ \AA}$  for Na). If the reactions observed<sup>45</sup> for K, Rb, and Cs proceed by harpooning, they must make use of an excited electronic state of  $\text{NO}_2^-$ . The lowest excited state is expected<sup>128,132</sup> to arise from raising one of the unshared electrons on the N atom to an antibonding  $\bar{\pi}$  orbital of the ion ( $n_{\text{N}} \rightarrow \bar{\pi}$ ). The results of the reactive scattering studies on  $\text{NO}_2$  and related compounds are not yet complete, but can be reasonably interpreted on this basis.<sup>45</sup> The primary product is a polar, paramagnetic molecule, almost certainly the MO molecule. In the  $\text{Na} + \text{NO}_2$  reaction, however, an additional diamagnetic contribution appears, which might be  $\text{NaNO}$  formed via the ground state of  $\text{NO}_2^-$ . For the analogous reactions of  $\text{CH}_3\text{NO}_2$ , the harpooning mechanism would be expected to use the ground state since the crossing radius would be pulled in (just as in the case of  $\text{CH}_3\text{I}$  compared to  $\text{I}_2$ ), and indeed the experiments show only a diamagnetic product.

The harpooning mechanism is a charming model for reactions which can proceed via ion-pair intermediates and it appears to be qualitatively correct. Further studies of the detailed mechanics of chemical reactions will surely lead to broader correlations with electronic structure. The success enjoyed by the valence theory of charge-transfer complexes<sup>113-115</sup> for a broad spectrum of cases in which the electron transfer is only partial is an encouraging example. In fact, a striking correspondence has been found<sup>134</sup> in comparing electron absorption coefficients estimated from gas chromatography<sup>135</sup> with rate constants for the large class of “reactions with inertia” studied in the Polanyi sodium flame experiments. This extends over a factor of  $10^4$  in reactivity. Perhaps there is good prospect for replacing the harpoon with a needle.

### Acknowledgments

The Berkeley and Harvard experiments listed in Table I extend over a very blissful period of five years. We have had no co-workers, but a working company: all of these experiments and much of the analysis presented here are due to G. H. Kwei, J. A. Norris, J. L. Kinsey, K. R. Wilson, R. R. Herm, J. H. Birely, E. A. Entemann, and M. C. Moulton. Support of the early work at Berkeley came primarily from the U. S. Atomic Energy Commission and that at Harvard from the National Science Foundation.

## References

1. T. H. Bull and P. B. Moon, *Discussions Faraday Soc.*, **17**, 54 (1954). Cs + CCl<sub>4</sub>; mechanically pulsed, accelerated beam, time-of-flight velocity analysis.
2. E. H. Taylor and S. Datz, *J. Chem. Phys.*, **23**, 1711 (1955). K + HBr; differential surface ionization method.
3. S. Datz and E. H. Taylor, in *Recent Research in Molecular Beams*, I. Estermann, Ed., Academic Press, New York, 1959, p. 157. Review of chemical applications of beam techniques.
4. R. W. Roberts, "The Scattering of a Potassium Atomic Beam by a Crossed Beam of Bromine Molecules," Ph.D. thesis, Brown University, Providence, Rhode Island, 1959.
5. E. F. Greene, R. W. Roberts, and J. Ross, *J. Chem. Phys.*, **32**, 940 (1960). Energy dependence of yield in K + HBr reaction.
6. D. R. Herschbach, *J. Chem. Phys.*, **33**, 1870 (1960). Kinematic limitations on reactive scattering of K + HBr.
7. D. R. Herschbach, G. H. Kwei, and J. A. Norris, *J. Chem. Phys.*, **34**, 1842 (1961). K + CH<sub>3</sub>I, K + C<sub>2</sub>H<sub>5</sub>I; anisotropy of recoil, internal excitation of products.
8. S. Datz, D. R. Herschbach, and E. H. Taylor, *J. Chem. Phys.*, **35**, 1549 (1961). Mechanics of crossed-beam reactions, analysis of K + HBr results.
9. H. Gienapp, *Z. Elektrochem.*, **65**, 417 (1961). K + Cl<sub>2</sub> and HI; influence of reactivity on total scattering cross section.
10. D. R. Herschbach, *Vortex*, **22**, 348 (1961). Review of reactive scattering experiments and analysis.
11. K. Kodera and T. Tamura, *Bull. Chem. Soc. Japan*, **34**, 566 (1961). Na + Cl<sub>2</sub>; total scattering cross section unaffected by reaction.
12. D. Beck, *J. Chem. Phys.*, **37**, 2884 (1962). Velocity selected K + Ar and HBr; rainbow scattering.
13. D. Beck, E. F. Greene, and J. Ross, *J. Chem. Phys.*, **37**, 2895 (1962). Velocity selected K + HBr; reaction probability derived from optical potential analysis of elastic scattering.
14. N. C. Blais and D. L. Bunker, *J. Chem. Phys.*, **37**, 2713 (1962). Monte Carlo computer study of K + CH<sub>3</sub>I reactive scattering.
15. D. R. Herschbach, *Discussions Faraday Soc.*, **33**, 149, 277, 278, 281 (1962). Restrictions imposed by conservation laws; review of reactive scattering of K, Rb, Cs with alkyl iodides.
16. J. Ross and E. F. Greene, *Proceedings of the Twelfth Solvay Conference* (1962); also, *Energy Transfer in Gases*, R. Stoops, Ed., Interscience, New York, 1964, p. 363. Review of studies of K + HBr, CH<sub>3</sub>Br and CH<sub>3</sub>I.
17. M. Ackerman, E. F. Greene, A. L. Moursund, and J. Ross, *Ninth International Symposium on Combustion*, Academic Press, Inc., New York, 1963. K + CH<sub>3</sub>Br, optical potential analysis of elastic scattering.
18. N. C. Blais and D. L. Bunker, *J. Chem. Phys.*, **39**, 315 (1963). Monte Carlo computer study of A + BC reactions.
19. S. Datz and E. H. Taylor, *J. Chem. Phys.*, **39**, 1896 (1963). D + H<sub>2</sub>; time-of-flight velocity analysis.

20. W. L. Fite and R. T. Brackmann, in *Atomic Collision Processes*, M. R. C. McDowell, Ed., North-Holland Pub. Co., Amsterdam, 1963, p. 955. H + D<sub>2</sub>.
21. W. L. Fite and S. Datz, *Ann. Rev. Phys. Chem.*, **14**, 61 (1963). General review of chemical research with beams.
22. E. Gersing, E. Hundhausen, and H. Pauly, *Z. Physik*, **171**, 349 (1963). Evidence for reaction in K + HgX<sub>2</sub> and SnI<sub>4</sub> scattering.
23. D. R. Herschbach and G. H. Kwei, in *Atomic Collision Processes*, M. R. C. McDowell, Ed., North-Holland Pub. Co., Amsterdam, 1963, p. 972. Model calculation of elastic scattering of reactive molecules.
24. J. A. Norris, "Chemical Reactions in Crossed Molecular Beams," Ph.D. thesis, University of California, Berkeley, 1963. Also, *UCRL Report, 10848*, Lawrence Radiation Laboratory, Berkeley, 1963.
25. M. Ackerman, E. F. Greene, A. L. Moursund, and J. Ross, *J. Chem. Phys.*, **41**, 1183 (1964). Velocity selected K + HCl and HI; optical potential analysis of elastic scattering.
26. D. L. Bunker, *Sci. Am.*, **211**, 100 (1964). Review of Monte Carlo computer studies of reaction dynamics.
27. D. L. Bunker and N. C. Blais, *J. Chem. Phys.*, **41**, 2377 (1964). Monte Carlo calculations extended to three-dimensional collisions.
28. S. Datz and R. E. Minturn, *J. Chem. Phys.*, **41**, 1153 (1964). Velocity selected Cs + Br<sub>2</sub>; stripping mechanism.
29. A. E. Grosser, A. R. Blythe, and R. B. Bernstein, *J. Chem. Phys.*, **42**, 1268 (1964). Velocity analysis of KBr from K + HBr.
30. R. Helbing and H. Pauly, *Z. Physik*, **179**, 16 (1964). Influence of reactivity on small-angle elastic scattering of K + Br<sub>2</sub> and several other halogen compounds.
31. R. R. Herm, R. Gordon, and D. R. Herschbach, *J. Chem. Phys.*, **41**, 2218 (1964). Magnetic deflection analysis of K + CH<sub>3</sub>I, Br<sub>2</sub>, and ICl scattering.
32. M. Karplus and L. Raff, *J. Chem. Phys.*, **41**, 1267 (1964). Monte Carlo method extended to three-dimensional collisions; study of K + CH<sub>3</sub>I; correlation between size of reaction cross section and anisotropy of angular distribution.
33. M. Karplus, R. N. Porter, and R. D. Sharma, *J. Chem. Phys.*, **40**, 2033 (1964). Monte Carlo computer study of D + H<sub>2</sub> reactive scattering.
34. J. C. Light, *J. Chem. Phys.*, **40**, 3221 (1964). Statistical theory of reactions.
35. A. L. Moursund, "The Elastic and Reactive Scattering of K by HCl, CH<sub>3</sub>Br, and HI in Crossed Molecular Beams," Ph.D. thesis, Brown University, Providence, Rhode Island, 1964.
36. R. J. Suplinskas, "Calculation of the Chemical Reaction Cross Section; K + HBr," Ph.D. thesis, Brown University, Providence, Rhode Island, 1964.
37. C. H. Williams, "The Dissociation of a Cesium Fluoride Molecule by Impact with a Fast Argon Atom," Ph.D. thesis, Brown University, Providence, Rhode Island, 1964.
38. K. R. Wilson, "Molecular Beam Studies of Chemical Dynamics," Ph.D. thesis, University of California, Berkeley, 1964. Also *UCRL Report, 11605*, Lawrence Radiation Laboratory, Berkeley, 1964.
39. K. R. Wilson, G. H. Kwei, J. A. Norris, R. R. Herm, J. H. Birely, and D. R. Herschbach, *J. Chem. Phys.*, **41**, 1154 (1964). K, Rb, Cs + Br<sub>2</sub>, I<sub>2</sub>, ICl, and IBr; stripping mechanism.

40. J. H. Birely, "Product Excitation in Reactive Scattering," Ph.D. thesis, Harvard University, Cambridge, Mass., 1965.
41. J. H. Birely and D. R. Herschbach, *J. Chem. Phys.*, **43** (1965). Velocity analysis of KBr from K + Br<sub>2</sub>.
42. J. H. Birely, R. R. Herm, K. R. Wilson, and D. R. Herschbach, *J. Chem. Phys.*, **43** (1965). K, Rb, Cs + Br<sub>2</sub> and I<sub>2</sub>.
43. E. F. Greene, A. L. Moursund, and J. Ross, this volume, p. 135. Review of elastic scattering of reactive molecules and optical potential analysis.
44. A. E. Grosser and R. B. Bernstein, *J. Chem. Phys.*, **43**, 1140 (1965). Velocity analysis of KBr from K + Br<sub>2</sub>.
45. R. R. Herm, "Electric and Magnetic Deflection Analysis of Reactive Scattering," Ph.D. thesis, Harvard University, Cambridge Mass., 1965. Also, *UCRL Reports 10526, 16039*, Lawrence Radiation Laboratory, Berkeley, 1962 and 1965.
46. R. R. Herm and D. R. Herschbach, *J. Chem. Phys.*, **43** (1965). Electric deflection analysis of K + Br<sub>2</sub> and Cs + HBr scattering; rotational excitation.
47. D. R. Herschbach, *Appl. Optics, Suppl. 2 (Chemical Lasers)*, **128** (1965). Review of alkali reactions, models for reaction dynamics.
48. J. L. Kinsey, G. H. Kwei, and D. R. Herschbach, *J. Chem. Phys.*, **43** (1965). Rb, Cs + alkyl iodides, optical potential model for rebound reactions.
49. G. H. Kwei, "Elastic and Reactive Scattering in Crossed Molecular Beams," Ph.D. thesis, University of California, Berkeley, 1965. Also, *UCRL Reports 11178, 11966*, Lawrence Radiation Laboratory, Berkeley, 1963 and 1965.
50. G. H. Kwei, J. A. Norris, and D. R. Herschbach, *J. Chem. Phys.*, **43** (1965). K + alkyl iodides; scattering kinematics.
51. P. Pechukas and J. C. Light, *J. Chem. Phys.*, **42**, 3281 (1965). Detailed balancing amendment to statistical theory.
52. P. Pechukas, J. C. Light, and C. Rankin, *J. Chem. Phys.*, **43** (1965). Statistical theory applied to atom exchange reactions.
53. R. G. J. Fraser, *Molecular Rays*, Cambridge University Press, Cambridge, 1931; *Molecular Beams*, Methuen, London, 1937.
54. N. F. Ramsey, *Molecular Beams*, Oxford University Press, Oxford, 1956.
55. P. Kusch and V. W. Hughes, in *Handbuch der Physik 37/1*, S. Flügge, Ed., Springer-Verlag, Heidelberg, 1959.
56. S. Datz and E. H. Taylor, *J. Chem. Phys.*, **25**, 389, 395 (1956).
57. K. R. Wilson and R. J. Ivanetich, *UCRL Repts. 10706, 11606*, Lawrence Radiation Laboratory, Berkeley, Cal., 1962 and 1965.
58. W. Schroen, *Z. Physik*, **176**, 237 (1963).
59. T. R. Touw and J. W. Trischka, *J. Appl. Phys.*, **34**, 3635 (1963).
60. Obtained from Linde Co., Crystal Products, 4120 Kennedy Ave., East Chicago, Indiana. A method of "growing" pure tungsten filaments has been described by E. F. Greene, *Rev. Sci. Instr.*, **32**, 860 (1961).
61. See, for example, R. B. Bernstein, *Science*, **144**, 141 (1964).
62. See, for example, J. P. Valteau and J. M. Deckers, *Can. J. Chem.*, **42**, 225 (1964).
63. E. Hundhausen and H. Pauly, Private communication (Bonn University, May, 1964).
64. R. A. Berg, L. Wharton, and W. Klemperer, *Bull. Am. Phys. Soc.*, **9**, 734 (1964);

- A. Büchler, J. L. Stauffer, W. Klemperer, and L. Wharton, *J. Chem. Phys.*, **39**, 2299 (1963).
65. E. A. Entemann, work in progress (Harvard University).
  66. M. Karplus, private communication (Columbia University).
  67. S. Datz and R. E. Minturn, private communication (Oak Ridge National Laboratory).
  68. H. U. Hostettler and R. B. Bernstein, *Rev. Sci. Instr.*, **31**, 872 (1960).
  69. H. G. Bennowitz, Dissertation, Physical Institute, Bonn, 1956.
  70. S. M. Trujillo, P. K. Rol, and E. W. Rothe, *Rev. Sci. Instr.*, **33**, 841 (1962).
  71. H. G. Bennowitz, K. H. Kramer, W. Paul, and J. P. Toennies, *Z. Physik*, **177**, 84 (1964).
  72. K. H. Kramer and R. B. Bernstein, *J. Chem. Phys.*, **42**, 767 (1965).
  73. J. P. Toennies, *Discussions Faraday Soc.*, **33**, 96 (1962); also in M. R. C. McDowell, Ed., *Atomic Collision Processes*, North-Holland Publishing Co., Amsterdam, 1963, p. 1113.
  74. See, for example, J. C. Polanyi, *J. Quant. Spectr. Radiative Transfer*, **3**, 481 (1963); also, J. V. V. Kasper and G. C. Pimentel, *Phys. Rev. Letters*, **14**, 352 (1965).
  75. M. C. Moulton, work in progress (Harvard University).
  76. T. L. Cottrell, *The Strengths of Chemical Bonds*, Butterworths, London, 1958.
  77. L. Brewer and E. Brackett, *Chem. Rev.*, **61**, 425 (1961).
  78. M. Polanyi, *Atomic Reactions*, Williams and Norgate, London, 1932.
  79. M. G. Evans and M. Polanyi, *Trans. Faraday Soc.*, **35**, 178 (1939).
  80. M. Krocsak and G. Schay, *Z. Physik. Chem. (Leipzig)*, **B19**, 344 (1932); E. Roth and G. Schay, *Ibid.*, **B28**, 323 (1935).
  81. S. Glasstone, K. J. Laidler, and H. Eyring, *Theory of Rate Processes*, McGraw-Hill, New York, 1941.
  82. J. L. Magee, *J. Chem. Phys.*, **8**, 687 (1940).
  83. For reviews of subsequent alkali flame studies see C. E. H. Bawn, *Ann. Rept. Chem. Soc.*, **39**, 36 (1943) and E. Warhurst, *Quart. Rev. Chem. Soc. (London)*, **5**, 44 (1951).
  84. V. N. Kondratiev, *Chemical Kinetics of Gas Reactions*, Pergamon Press, London 1964, p. 87.
  85. J. C. Polanyi, *J. Chem. Phys.*, **31**, 1338 (1959).
  86. N. Basco and R. G. W. Norrish, *Can. J. Chem.*, **38**, 1769 (1960).
  87. B. S. Rabinovitch and M. C. Flowers, *Quart. Rev. Chem. Soc. (London)*, **18**, 122 (1964).
  88. K. E. Shuler, T. Carrington, and J. C. Light, *Appl. Optics*, **Suppl. 2 (Chemical Lasers)**, 81 (1965).
  89. J. C. Polanyi, *Appl. Optics*, **Suppl. 2 (Chemical Lasers)**, 109 (1965).
  90. F. Kaufman, *Discussions Faraday Soc.* **33**, 138, 284, (1962).
  91. J. R. Airey, R. R. Getty, J. C. Polanyi, and D. R. Snelling, *J. Chem. Phys.*, **41**, 3255 (1964).
  92. F. T. Smith, *J. Chem. Phys.*, **31**, 1352 (1959).
  93. J. Simons, *Nature*, **186**, 551 (1960).
  94. D. L. Bunker, *Nature*, **194**, 1277 (1962).
  95. See, for example, R. M. Eisberg and C. E. Porter, *Rev. Mod. Phys.*, **33**, 190 (1961).

96. K. W. Ford and J. A. Wheeler, *Ann. Phys. (N. Y.)*, **7**, 259 (1959).
97. See, for example, B. H. Mahan, *J. Chem. Phys.*, **32**, 362 (1960); K. Yang and T. Ree, *J. Chem. Phys.*, **35**, 588 (1961); H. S. Johnston and P. Goldfinger, *J. Chem. Phys.*, **37**, 700 (1962); and references cited therein.
98. H. O. Pritchard, *Chem. Rev.*, **52**, 529 (1953).
99. F. H. Field and J. L. Franklin, *Electron Impact Phenomena*, Academic Press, New York, 1957, p. 148.
100. L. M. Branscomb, *Advan. Electron Phys.*, **9**, 43 (1957); *Atomic and Molecular Processes*, D. R. Bates, Ed., Academic Press, New York, 1962, p. 100.
101. W. B. Person, *J. Chem. Phys.*, **38**, 109 (1963).
102. See, for example, W. Kauzmann, *Quantum Chemistry*, Academic Press, New York, 1957, p. 536.
103. R. S. Berry, *J. Chem. Phys.*, **27**, 1288 (1957).
104. E. Teller, *J. Phys. Chem.*, **41**, 109 (1937); G. Herzberg and H. C. Longuet-Higgins, *Discussions Faraday Soc.*, **35**, 77 (1963).
105. J. C. Slater and J. G. Kirkwood, *Phys. Rev.*, **37**, 682 (1931).
106. E. S. Rittner, *J. Chem. Phys.*, **19**, 1030 (1951).
107. A. C. Riviere and D. R. Sweetman, *Phys. Rev. Letters*, **5**, 560 (1960); H. Wind, *Proc. Phys. Soc. (London)*, **84**, 617 (1964).
108. J. R. Hiskes, *Phys. Rev.*, **122**, 1207 (1961); *Nucl. Fission*, **2**, 38 (1962).
109. J. C. Polanyi, private communication (University of Toronto).
110. S. T. Butler, *Nuclear Stripping Reactions*, Wiley, New York, 1957.
111. See, for example, C. A. Levinson and M. K. Banerjee, in F. Ajzenberg-Selove, Ed., *Nuclear Spectroscopy*, Academic Press, New York, 1960, Chap. VB.
112. A. Henglein and G. A. Muccini, *Z. Naturforsch.*, **17a**, 452 (1962); **18a**, 753 (1963); A. Henglein, K. Lacmann, and G. Jacobs, *Ber. Bunsenges. Physik. Chem.*, **69**, 279, 286, 292 (1965).
113. R. S. Mulliken, *J. Am. Chem. Soc.*, **74**, 811 (1950).
114. G. Briegleb, *Elektron-Donator-Acceptor Komplexe*, Springer-Verlag, Berlin, 1961.
115. R. S. Mulliken, *J. Chim. Phys.*, **61**, 20 (1963).
116. R. N. Zare and D. R. Herschbach, *J. Mol. Spectry*, **15**, 462 (1965).
117. R. S. Mulliken, *J. Am. Chem. Soc.*, **72**, 600 (1950); **77**, 884 (1955).
118. R. S. Berry and C. W. Reimann, *J. Chem. Phys.*, **38**, 1540 (1963).
119. A. G. Gaydon, *Dissociation Energies*, Chapman and Hall, London, 2nd Ed., 1953, p. 45.
120. C. J. Delbecq, W. Hayes, and P. H. Yuster, *Phys. Rev.*, **121**, 1043 (1961); *Proc. Roy. Soc. (London)*, **A271**, 243 (1963).
121. G. Dobson and L. I. Grossweiner, *Radiation Res.*, **23**, 290 (1964) and earlier papers cited therein.
122. M. A. Biondi and R. E. Fox, *Phys. Rev.*, **109**, 2012 (1958).
123. D. C. Frost and C. A. McDowell, *J. Chem. Phys.*, **29**, 964 (1958); *Can. J. Chem.*, **38**, 407 (1960).
124. See, for example, R. I. Reed, *Ion Production by Electron Impact*, Academic Press, New York, 1962, pp. 87 and 116; C. A. McDowell, *Mass Spectrometry*, McGraw-Hill, New York, 1963, p. 526.

125. V. M. Dukelskii and V. M. Sokolov, *J. Exptl. Theoret. Phys. (USSR)*, **32**, 394 (1957); S. Buchel'nikova, *ibid.*, **34**, 519 (1959).
126. G. H. Dunn, *Phys. Rev. Letters*, **8**, 62 (1962).
127. R. N. Zare and D. R. Herschbach, *Proc. I.E.E.E.*, **51**, 173 (1963); *Appl. Optics Suppl.*, **2**, 193 (1965).
128. A. D. Walsh, *J. Chem. Soc.*, **1953**, 2260.
129. R. S. Mulliken, *Phys. Rev.*, **47**, 413 (1935).
130. G. Herzberg, *Discussions Faraday Soc.*, **35**, 7 (1963).
131. D. C. Frost and C. A. McDowell, *J. Chem. Phys.*, **29**, 503 (1958).
132. W. G. Trawick and W. H. Eberhardt, *J. Chem. Phys.*, **22**, 1462 (1954).
133. R. K. Curran, *Phys. Rev.*, **125**, 910 (1962).
134. K. R. Wilson and D. R. Herschbach, *Nature*, **207** (1965).
135. J. E. Lovelock and N. L. Gregory in N. Brenner, J. E. Callear, and M. D. Weiss, Eds., *Gas Chromatography*, Academic Press, New York, 1962, p. 227; J. E. Lovelock, *Anal. Chem.*, **35**, 474 (1963).